submitted to *Geophys. J. Int.*

3-D Projected L_1 inversion of gravity data

Saeed Vatankhah [1], Rosemary A. Renaut [2] and Vahid E. Ardestani [1]

[1] *Institute of Geophysics, University of Tehran, Iran*

[2] *School of Mathematical and Statistical Sciences, Arizona State University, Tempe, AZ, USA.*

SUMMARY

Sparse inversion of the large scale gravity problem is considered. The L_1-type stabilizer reconstructs models with sharp boundaries and blocky features, and is implemented here using an iteratively reweighted L_2-norm (IRLS). The resulting large scale regularized least squares problem at each iteration is solved on the projected subspace obtained using Golub-Kahan iterative bidiagonalization applied to the large scale linear system of equations. The regularization parameter for the IRLS problem is estimated using the unbiased predictive risk estimator (UPRE) extended for the projected problem. Further analysis leads to an improvement of the projected UPRE via analysis based on truncation of the projected spectrum. Numerical results for synthetic examples and real field data demonstrate the efficiency of the method.

Key words: Inverse theory; Numerical approximation and analysis; Gravity anomalies and Earth structure; Asia

1 INTRODUCTION

The gravity data inversion problem is the estimation of the unknown subsurface density and its geometry from a set of gravity observations measured on the surface. This is a challenging problem for several reasons: Foremost of these is the non-uniqueness of the problem, there are fewer observations than the number of model parameters yielding algebraic ambiguity, but also by Gauss's theorem non-uniqueness arises due to the physics of the problem, (Li & Oldenburg 1996). Further, the data are

always contaminated with noise, which, with the ill-conditioning of the model, leads to sensitivity of the solution to the noise and to the numerical algorithm for finding the solution. Thus, the inversion of gravity data is an example of an under-determined and ill-posed problem, for which a stable and geologically plausible solution is feasible only with the imposition of additional information on the model. Here we consider the minimization of a global objective function consisting of data misfit, $\Phi(\mathbf{m})$, and stabilizing regularization, $S(\mathbf{m})$, terms, with relative weighting determined by regularization parameter α,

$$P^{\alpha}(\mathbf{m}) = \Phi(\mathbf{m}) + \alpha^2 S(\mathbf{m}). \tag{1}$$

Data misfit $\Phi(\mathbf{m})$ measures how well an obtained model, $\mathbf{m}$, reproduces the observed data, $\mathbf{d}_{\rm obs}$. For gravity data it is standard to assume that the noise in the data is uncorrelated and Gaussian, although it arises due to several sources such as untreated instrumental or geologic noise. Assuming that the standard deviation of the noise in the data is known, then a weighted L_2 measure of the error between the observed and the predicted data is used giving $\Phi(\mathbf{m}) = \|W_{\mathbf{d}}(G\mathbf{m} - \mathbf{d}_{\rm obs})\|_2^2$, where $W_{\mathbf{d}}$ is a diagonal matrix approximating the inverse of the diagonal standard deviation matrix of the data. We note that throughout we use the standard definition $\|\mathbf{x}\|_p$ to be the L_p-norm of vector $\mathbf{x}$, given by $\|\mathbf{x}\|_p = (\sum_{i=1}^{n} |x_i|^p)^{\frac{1}{p}}, p \geq 1$.

There are several choices for the stabilizer, $S(\mathbf{m})$, depending on the type of features one wants to see from the inverted model. A typical choice for geophysical applications is given by $S(\mathbf{m}) = \|W_{\mathbf{m}}(\mathbf{m} - \mathbf{m}_{\rm apr})\|_2^2$ in which $\mathbf{m}_{\rm apr}$ may be some prior information on the model, and $W_{\mathbf{m}}$ is an augmented matrix of spatially dependent weighting matrices, including potentially a depth weighting matrix and matrices that approximate low order derivative operators in each dimension, (Li & Oldenburg 1996, (4)). Then (1) involves two quadratic terms, and, supposing that the null spaces of both G and $W_{\mathbf{m}}$ intersect only trivially, the unique minimizer of $P^{\alpha}(\mathbf{m})$ is obtained as the solution of a linear system, the *normal equations*, for (1). Although this type of inversion has been used successfully in much geophysical literature, models recovered in this way are characterized by smooth features, especially blurred boundaries, which are not always consistent with real geological structures (Farquharson 2008). There are situations in which the sources are localized and separated by sharp, distinct interfaces, requiring alternative approaches. In the geophysical community, Last & Kubik (1983) presented a compactness criterion for gravity inversion that seeks to minimize the area (or volume in 3D) of the causative body. In this case, $\mathbf{m}_{\rm apr} = 0$ and $W_{\mathbf{m}}(\mathbf{m}) = W_{\epsilon}(\mathbf{m}) = \mathrm{diag}(1/(\mathbf{m}^2 + \epsilon^2)^{1/2})$, for small $\epsilon > 0$, i.e. $S(\mathbf{m}) = \|W_{\epsilon}(\mathbf{m})\mathbf{m}\|_2^2$. Now, (1) is a non-linear function of $\mathbf{m}$, and the model-space iteratively reweighted least square (IRLS) algorithm is used to solve the problem. At each iteration k, $\mathbf{m}^{(k)}$ is obtained using the weighting matrix $W_{\epsilon}^{(k)}(\mathbf{m})$ calculated using $\mathbf{m}^{(k-1)}$, where for any variable the

superscript $^{(k)}$ denotes that variable at iteration k, and here we assume $W_\epsilon^{(1)}(\mathbf{m}) = I$. Incorporating $\mathbf{m}_{\rm apr}$ into the stabilizer, i.e. $S(\mathbf{m}) = \|W_\epsilon(\mathbf{m})(\mathbf{m} - \mathbf{m}_{\rm apr})\|_2^2$ with now $W_\epsilon(\mathbf{m})$ defined by

$$W_\epsilon(\mathbf{m}) = \mathrm{diag}(1/((\mathbf{m} - \mathbf{m}_{\rm apr})^2 + \epsilon^2)^{1/2}), \tag{2}$$

gives the minimum support (MS) stabilizer which minimizes the total volume of nonzero departure of the model parameters from the given prior model, (Portniaguine & Zhdanov 1999). A further modification introduced in (Portniaguine & Zhdanov 1999) uses the gradient of the model parameters in the stabilization term via $S(\mathbf{m}) = \|D_\epsilon(\nabla\mathbf{m})|\nabla\mathbf{m}|\|_2^2$, where $D_\epsilon(\nabla\mathbf{m})$ is defined by $\mathrm{diag}(1/(|\nabla\mathbf{m}|^2 + \epsilon^2)^{1/2})$, yielding the minimum gradient support (MGS) stabilizer. This constraint minimizes the volume over which the gradient of the model parameters is nonzero, and thus yields models with sharp boundaries.

Another possibility for the reconstruction of sparse models is to use a stabilizer which minimizes the L_1-norm of the model or gradient, in this case known as the total variation (TV), of the model parameters (Farquharson & Oldenburg 1998; Farquharson 2008; Loke et al. 2003). The L_1-norm stabilizer permits occurrence of large elements in the inverted model among mostly small values and can, therefore, be used to obtain models with non-smooth properties (Sun & Li 2014). Although the L_1-norm stabilizer has favorable properties, and yields a convex functional that can be solved by linear programming algorithms, its use for the solution of large scale problems is not feasible. Here we implement the L_1-norm stabilizer using the approximation based on an IRLS algorithm, (Bruckstein et al. 2009), and extend the algorithm for the gravity inverse problem by including the depth weighting and prior model information. Further, we use the weighting matrix similar to that used for the MS stabilizer but defined by

$$W_{L_1}(\mathbf{m}) = \mathrm{diag}(1/((\mathbf{m} - \mathbf{m}_{\rm apr})^2 + \epsilon^2)^{1/4}), \tag{3}$$

where we point to the use of fourth root in the denominator rather than square root in (2). Our results will compare these choices.

Many techniques have been developed to estimate a suitable regularization parameter, α in (1), including the L-curve (LC) (Hansen 1992), and Generalized Cross Validation (GCV) (Golub et al. 1979; Marquardt 1970), and methods which assume some knowledge of the noise level of the data, including the χ^2-discrepancy principle (Mead & Renaut 2009; Renaut et al. 2010; Vatankhah et al. 2014b), the unbiased predictive risk estimator (UPRE) (Vogel 2002) and the Morozov discrepancy principle (MDP) (Morozov 1966). Our previous investigation for the gravity inverse problem, see Vatankhah et al (2015), has demonstrated that the UPRE parameter-choice method provides a good estimate for the Tikhonov regularization parameter especially for high noise levels. Therefore, here,

we use the UPRE for estimation of the regularization parameter α, extending the approach in (Renaut et al. 2015).

For small-scale problems involving two quadratic terms the solution of (1) may be found efficiently using the generalized singular value decomposition (GSVD) or singular value decomposition (SVD), dependent on the choice for $W_{\mathbf{m}}$. In addition, these factorizations present regularization parameter-choice methods in computationally convenient forms (Vatankhah et al. 2014b). For large-scale problems these factorizations are generally computationally impractical and an alternative approach is to find the solution through projection of the problem to a smaller subspace, on which it may then be feasible to use the factorization for efficient estimation of the regularization parameter. Here we use the Golub-Kahan iterative bidiagonalization projection of the solution which is based on the LSQR Krylov methods introduced in Paige & Saunders (1982a; 1982b). Then, effective parameter estimation techniques, that are useful in the context of efficient iterative Krylov-based procedures, must be developed. Chung et al. presented the weighted GCV for the projected problem which requires the use of an additional solution dependent weighting parameter, (Chung et al. 2008). Here we focus our discussion on the UPRE in conjunction with the solution of the projected problem, additionally extending the approach introduced in (Renaut et al. 2015).

The outline of this paper is as follows. In Section 2 we review the inversion algorithm and transformation of the L_1-norm stabilizer into the standard form Tikhonov functional. Furthermore, the development of the Tikhonov regularization functional based on the Golub-Kahan iterative bidiagonalization is given in Section 2.1. Section 3 is devoted to discussion of parameter estimation, the derivation of the UPRE is presented in Section 3.1 with new work showing its extension for usage with the projected problem in Section 3.2. Results for synthetic examples are illustrated in Section 4. The reconstruction of an embedded cube with high density within a homogeneous medium is used for contrasting the algorithms using the SVD, Section 4.2 and the LSQR algorithm, Section 4.3. These results demonstrate the need to use the truncated UPRE which is introduced and applied in Section 4.4. The reconstruction of a more complex structure using the TUPRE is presented in Section 4.5. These simulations are concluded with the contrast of the MS and L_1 stabilizers in Section 4.6. The approach is applied on gravity data acquired over a hematite mine located in the southeast of Iran and the results are shown in Section 5. Conclusions and future work follow in Section 6.

2 L_1 INVERSION METHODOLOGY

We briefly review the well-known approach for the standard 3D inversion of gravity data. The subsurface volume is discretized using a set of cubes, in which the cells size are kept fixed during the inversion, and the values of densities at the cells are the model parameters to be determined in the

inversion (Boulanger & Chouteau 2001; Li & Oldenburg 1998). Thus, we can introduce a vector $\mathbf{m}$ of the unknown model parameters, here the density of each cell ρ_j, such that $\mathbf{m} = (\rho_1, \rho_2, \ldots, \rho_n) \in \mathcal{R}^n$ and a vector $\mathbf{d}_{\rm obs} \in \mathcal{R}^m$ which contains the measured data. Then, the gravity data satisfy the rectangular underdetermined linear system

$$\mathbf{d}_{\rm obs} = G\mathbf{m}. \tag{4}$$

Practically, $\mathbf{d}_{\rm obs} = \mathbf{d}_{\rm exact} + \boldsymbol{\eta}$, where $\mathbf{d}_{\rm exact}$ is the unknown exact data and $\boldsymbol{\eta} \in \mathcal{R}^m$ represents the error in the measurements, assumed to be Gaussian and uncorrelated. The matrix $G \in \mathcal{R}^{m\times n}, m \ll n$, is the matrix resulting from the discretization of the forward operator which maps from the model space to the data space. Given G, the goal of the gravity inverse problem is to find a stable and geologically plausible density model $\mathbf{m}$ that reproduces $\mathbf{d}_{\rm obs}$ at the noise level.

As discussed in section 1, solving problem (4) is challenging due to the ill-posed nature of the problem and regularization is required to stabilize the solution. Furthermore, depth weighting and prior model information should be included in the formulation. Rewriting (4) via $\mathbf{d}_{\rm obs} - G\mathbf{m}_{\rm apr} = G\mathbf{m} - G\mathbf{m}_{\rm apr}$ and then introducing the residual and discrepancy from the background data, using $\mathbf{r} = \mathbf{d}_{\rm obs} - G\mathbf{m}_{\rm apr}$ and $\mathbf{y} = \mathbf{m} - \mathbf{m}_{\rm apr}$, respectively, for which it is immediate that $\mathbf{r} = G\mathbf{y}$, we obtain the functional for $\mathbf{y}$,

$$P^{\alpha}(\mathbf{y}) = \|W_{\mathbf{d}}(G\mathbf{y} - \mathbf{r})\|_2^2 + \alpha^2\|\mathbf{y}\|_1, \tag{5}$$

here introducing the L_1 regularization term. Assuming minimization of (5) to give $\mathbf{y}(\alpha)$, the model is updated by $\mathbf{m}(\alpha) = \mathbf{m}_{\rm apr} + \mathbf{y}(\alpha)$. In the IRLS algorithm $\|\mathbf{y}\|_1$ is approximated as follows. We first note, following for example (Voronin 2012; Wohlberg & Rodriguez 2007), that $|y_i| = y_i^2/\sqrt{y_i^2}$ can be approximated by $y_i^2/\sqrt{y_i^2 + \epsilon^2}$ for small and positive ϵ. Thus

$$\|\mathbf{y}\|_1 \approx \sum_{i=1}^{n} \frac{y_i^2}{\sqrt{y_i^2 + \epsilon^2}} = \sum_{i=1}^{n} (W_{L_1})_{ii}^2\, y_i^2 = \|W_{L_1}(\mathbf{y})\mathbf{y}\|^2, \text{ for } (W_{L_1}(\mathbf{y}))_{ii} = \frac{1}{(y_i^2 + \epsilon^2)^{1/4}},$$

and (5) is replaced by the approximating differentiable functional with diagonal matrix $W_{L_1}(\mathbf{y})$,

$$P^{\alpha}(\mathbf{y}) = \|W_{\mathbf{d}}(G\mathbf{y} - \mathbf{r})\|_2^2 + \alpha^2\|W_{L_1}(\mathbf{y})\mathbf{y}\|_2^2, \quad \mathbf{y} = (\mathbf{m} - \mathbf{m}_{\rm apr}). \tag{6}$$

Now the close relationship between the MS and L_1-norm stabilizers is clear, the difference being the fractional root, as is seen by introducing

$$S_p(\mathbf{x}) = \sum_{i=1}^{n} e_p(x_i) \quad \text{where} \quad e_p(x) = \frac{x^2}{(x^2 + \epsilon^2)^{\frac{2-p}{2}}}. \tag{7}$$

When ϵ is sufficiently small, (7) yields the approximation of the L_p norm for $p = 2$ and $p = 1$, while the case with $p = 0$ corresponds to the compactness constraint used in Last & Kubik (1983). $S_0(\mathbf{x})$ does not meet the mathematical requirement to be regarded as a norm, and is commonly used

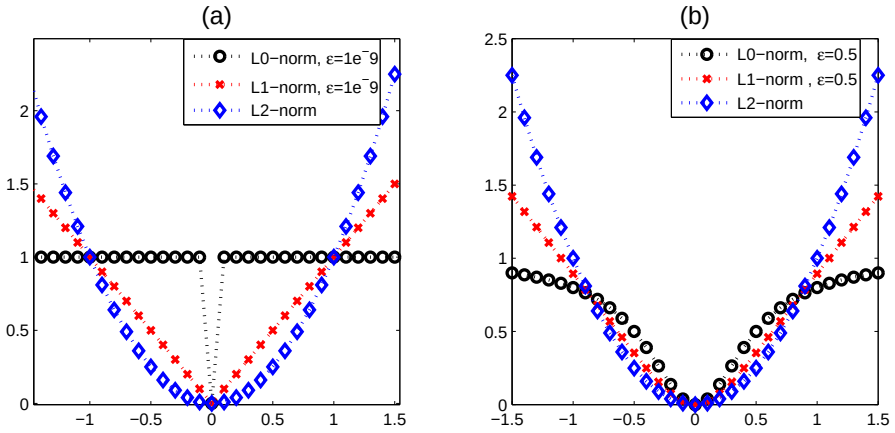

Figure 1. Illustration of different norms for two values of parameter ϵ. (a) $\epsilon = 1e{-}9$; (b) $\epsilon = 0.5$.

to denote the number of nonzero entries in $\mathbf{x}$. Fig. 1 demonstrates the impact of the choice of ϵ on $e_p(x)$ for $\epsilon = 1e^{-9}$, Fig. 1(a), and $\epsilon = 0.5$, Fig. 1(b). For larger p, more weight is imposed on large elements of $\mathbf{x}$, large elements will be penalized more heavily than small elements during minimization (Sun & Li 2014). Hence L_2 tends to discourage the occurrence of large elements in the inverted model, yielding smooth models, while L_1 and L_0 allow large elements leading to the recovery of data with blocky features. Further, the L_0-norm is non-quadratic and $e_0(x)$ asymptotes to one away from 0, regardless of the magnitude of x. Hence the penalty on the model parameters does not depend on their relative magnitude, only on whether or not they lie above or below a threshold dependent on ϵ (Ajo-Franklin et al. 2007). Further, L_1 does not necessarily lead to a very sparse solution and thus L_0 is better for preserving sparsity. On the other hand, as compared to L_1, the disadvantage of L_0 is the greater dependency on the choice of ϵ, so that it is less robust than L_1.

Now, incorporating diagonal matrix $W_{\rm z}$, where we generally assume that this is a depth weighting matrix, into (6), see Li & Oldenburg (1998), yields

$$P^{\alpha}(\mathbf{y}) = \|W_{\mathbf{d}}(G\mathbf{y} - \mathbf{r})\|_2^2 + \alpha^2 \|W_{L_1}(\mathbf{y}) W_{\rm z}\mathbf{y}\|_2^2, \tag{8}$$

with model dependent weighting in the regularization term, $W(\mathbf{y}) = W_{L_1}(\mathbf{y})W_{\rm z}$. Thus the IRLS algorithm can be used to find a solution to the inverse problem as follows. The normal equations for (8), for given W, now dropping the dependence on $\mathbf{y}$, with $\tilde{G} = W_{\mathbf{d}}G$ and $\tilde{\mathbf{r}} = W_{\mathbf{d}}\mathbf{r}$, yield

$$\mathbf{y}(\alpha) = (\tilde{G}^T\tilde{G} + \alpha^2 W^T W)^{-1}\tilde{G}^T\tilde{\mathbf{r}}.$$

For $\epsilon > 0$, W is invertible and (8) can be transformed to standard form using

$$(\tilde{G}^T\tilde{G} + \alpha^2 W^T W) \;\; = \;\; W^T((W^T)^{-1}\tilde{G}^T\tilde{G}W^{-1} + \alpha^2 I_n)W = W^T(\tilde{\tilde{G}}^T\tilde{\tilde{G}} + \alpha^2 I_n)W,$$

with $\tilde{\tilde{G}} = \tilde{G}W^{-1}$, which corresponds to variable preconditioning of $\tilde{G}$. Now the standard Tikhonov

functional for the left and right preconditioned system is given by

$$P^{\alpha}(\mathbf{h}) = \|\tilde{\tilde{G}}\mathbf{h} - \tilde{\mathbf{r}}\|_2^2 + \alpha^2\|\mathbf{h}\|_2^2, \quad \text{where} \quad \mathbf{h}(\alpha) = W\mathbf{y}(\alpha). \tag{9}$$

Solution

$$\mathbf{h}(\alpha) = (\tilde{\tilde{G}}^T\tilde{\tilde{G}} + \alpha^2 I_n)^{-1}\tilde{\tilde{G}}^T\tilde{\mathbf{r}} = \tilde{\tilde{G}}(\alpha)\tilde{\mathbf{r}}, \quad \text{where} \quad \tilde{\tilde{G}}(\alpha) = (\tilde{\tilde{G}}^T\tilde{\tilde{G}} + \alpha^2 I_n)^{-1}\tilde{\tilde{G}}^T, \tag{10}$$

yields the model update $\mathbf{m}(\alpha) = \mathbf{m}_{\text{apr}} + W^{-1}\mathbf{h}(\alpha)$. For small-scale problems, the numerical solutions of (10) can be obtained using the SVD for $\tilde{\tilde{G}}$, see appendix A. Practically, however, within the context of the IRLS in which W, and hence $\tilde{\tilde{G}}$, are updated each step, the computation of the SVD each step still represents a significant overhead for the iterative algorithm. For the forthcoming discussion on the solution of large scale problems the overhead of the iterative update for $\tilde{\tilde{G}}$ is insignificant. While for clarity in Algorithm 1 we directly form $\tilde{\tilde{G}}$, we note that for some cases where G has certain structure that may be eliminated by the pre and post multiplication even by diagonal matrices W_{z} and W_{L_1}, it is possible and efficient to consider the matrix vector products of $\tilde{\tilde{G}}\mathbf{x}$ for arbitrary $\mathbf{x}$ without explicitly forming $\tilde{\tilde{G}}$, as discussed in (Renaut et al. 2015). We note that in such cases when W_{z} and W_{L_1} are diagonal, multiplication, inversion and storage requirements are minimal, of $\mathcal{O}(n)$ only.

Application of the IRLS for the solution of the inverse problem requires the designation of a termination test to determine whether or not an acceptable solution has been reached. Two criteria are chosen to terminate the algorithm; either the solution satisfies the noise level,

$$\chi^2_{\text{Computed}} = \|\frac{(\mathbf{d}_{\text{obs}})_i - (G\mathbf{m})_i}{\boldsymbol{\eta}_i}\|_2^2 \leq m + \sqrt{2m}, \tag{11}$$

or a maximum number of iterations, $K_{\max}$, is reached. Additionally, at each step practical lower and upper bounds on the density, $[\rho_{\min}, \rho_{\max}]$, are imposed to recover reliable subsurface models. If at any iterative step a given density value falls outside the bounds, the value at that cell is projected back to the nearest constraint value. At iteration k we use the approximation of (7) given by

$$e_p(x^{(k)}, x^{(k-1)}) = \frac{(x^{(k)})^2}{((x^{(k-1)})^2 + \epsilon^2)^{(\frac{2-p}{2})}}, \tag{12}$$

where $x^{(k)}$ denotes the unknown model parameter. Typically, as the iterations proceed, if $x^{(k)}$ converges, the approximation of (7) by (12) is increasingly better. The IRLS algorithm for small scale L_1 inversion is summarized in Algorithm 1.

2.1 Numerical solution by the Golub-Kahan bidigonalization

It is not viable to use the SVD decomposition for large scale problems, rather iterative methods such as conjugate gradients (CG), or other Krylov methods, can be employed to find $\mathbf{h}(\alpha)$. In any case, however, the problem of finding the optimal parameter α is a further complication. In general deter-

Algorithm 1 Iterative L_1 Inversion Algorithm

Input: $\mathbf{d}_{\rm obs}$, $\mathbf{m}_{\rm apr}$, G, $W_{\mathbf{d}}$, $\epsilon > 0$, $\rho_{\min}$, $\rho_{\max}$, $K_{\max}$

1: Calculate $W_{\rm z}$, $\tilde{G} = W_{\mathbf{d}}G$, and $\tilde{\mathbf{d}}_{\rm obs} = W_{\mathbf{d}}\mathbf{d}_{\rm obs}$

2: Initialize $\mathbf{m}^{(0)} = \mathbf{m}_{\rm apr}$, $W_{L_1}^{(1)} = I_n$, $W^{(1)} = W_{\rm z}$

3: Calculate $\tilde{\mathbf{r}}^{(1)} = \tilde{\mathbf{d}}_{\rm obs} - \tilde{G}\mathbf{m}^{(0)}$, $\tilde{\tilde{G}}^{(1)} = \tilde{G}(W^{(1)})^{-1}$, $k = 0$

4: **while** Not converged, (11) not satisfied, and $k < K_{\max}$ **do**

5: $k = k + 1$

6: Find the SVD: $\tilde{\tilde{G}}^{(k)} = U\Sigma V^T$

7: Use regularization parameter estimation to find $\alpha^{(k)}$

8: Set $\mathbf{h}^{(k)} = \sum_{i=1}^{m} \frac{\sigma_i^2}{\sigma_i^2+(\alpha^{(k)})^2} \frac{\mathbf{u}_i^T\tilde{\mathbf{r}}^{(k)}}{\sigma_i}\mathbf{v}_i$

9: Set $\mathbf{m}^{(k)} = \mathbf{m}^{(k-1)} + (W^{(k)})^{-1}\mathbf{h}^{(k)}$

10: Impose constraint conditions on $\mathbf{m}^{(k)}$ to force $\rho_{\min} \leq \mathbf{m}^{(k)} \leq \rho_{\max}$

11: Calculate the residual $\tilde{\mathbf{r}}^{(k+1)} = \tilde{\mathbf{d}}_{\rm obs} - \tilde{G}\mathbf{m}^{(k)}$

12: Set $W_{L_1}^{(k+1)} = \text{diag}\left(\left((\mathbf{m}^{(k)} - \mathbf{m}^{(k-1)})^2 + \epsilon^2\right)^{-1/4}\right)$, as in (3), and $W^{(k+1)} = W_{L_1}^{(k+1)}W_{\rm z}$

13: Calculate $\tilde{\tilde{G}}^{(k+1)} = \tilde{G}(W^{(k+1)})^{-1}$

14: **end while**

Output: Solution $\rho = \mathbf{m}^{(k)}$. $K = k$.

mination of an optimal α requires calculating $\mathbf{h}(\alpha)$ for multiple α. Alternatively, as suggested for example in Chung et al. (2008) and Kilmer & O'Leary (2001), regularization may be imposed on a smaller space. The Golub-Kahan bidiagonalization (GKB) is applied to project the solution of the inverse problem to a smaller subspace. If we apply t steps of the GKB on matrix $\tilde{\tilde{G}}$ with initial vector $\tilde{\mathbf{r}}$, then bidiagonal matrix $B_t \in \mathcal{R}^{(t+1)\times t}$ and matrices $H_{t+1} \in \mathcal{R}^{m\times(t+1)}$, $A_t \in \mathcal{R}^{n\times t}$ with orthonormal columns will be generated such that, see (Hansen 2007; Kilmer & O'Leary 2001),

$$\tilde{\tilde{G}}A_t = H_{t+1}B_t, \quad H_{t+1}\mathbf{e}_{t+1} = \tilde{\mathbf{r}}/\|\tilde{\mathbf{r}}\|_2.$$

For further discussion we explicitly use the subscript to indicate that the unit vector here is of length $(t+1)$ with a 1 in the first entry. The columns of A_t form an orthonormal basis for the Krylov subspace

$$K_t(\tilde{\tilde{G}}^T\tilde{\tilde{G}}, \tilde{\tilde{G}}^T\tilde{\mathbf{r}}) = \text{span}\{\tilde{\tilde{G}}^T\tilde{\mathbf{r}}, (\tilde{\tilde{G}}^T\tilde{\tilde{G}})\tilde{\tilde{G}}^T\tilde{\mathbf{r}}, \ldots, (\tilde{\tilde{G}}^T\tilde{\tilde{G}})^{t-1}\tilde{\tilde{G}}^T\tilde{\mathbf{r}}\}, \tag{13}$$

and an approximate solution $\mathbf{h}_t$ that lies in this Krylov subspace will have the form $\mathbf{h}_t = A_t\mathbf{z}_t$, $\mathbf{z}_t \in \mathcal{R}^t$. Note, we denote the quantities obtained using t steps of the factorization always with subscript t. The matrix W^{-1}, which acts as a right-preconditioner for the system, must be updated at each iteration k (the same happens for $\tilde{\mathbf{r}}$) and then the Krylov subspace (13) is changed at each iteration. Here the

preconditioner is not used to accelerate convergence, but it is used to enforce some specific regularity condition on the solution (Gazzola & Nagy 2014).

We now introduce notation that will be helpful in the discussion for estimation of the regularization parameter. Specifically, defining the residuals for the full problem and projected problems by, respectively,

$$\mathbf{R}_{\text{full}}(\mathbf{h}_t) = \tilde{\tilde{G}}\mathbf{h}_t - \tilde{\mathbf{r}}, \quad \text{and} \quad \mathbf{R}_{\text{proj}}(\mathbf{z}_t) = B_t\mathbf{z}_t - \|\tilde{\mathbf{r}}\|_2\mathbf{e}_{t+1}, \tag{14}$$

then

$$\mathbf{R}_{\text{full}}(\mathbf{h}_t) = \tilde{\tilde{G}}A_t\mathbf{z}_t - \tilde{\mathbf{r}} = H_{t+1}B_t\mathbf{z}_t - H_{t+1}\|\tilde{\mathbf{r}}\|_2\mathbf{e}_{t+1} = H_{t+1}\mathbf{R}_{\text{proj}}(\mathbf{z}_t).$$

By the column orthogonality of H_{t+1} it is immediate that the fidelity norm is preserved under projection, $\|\mathbf{R}_{\text{full}}(\mathbf{h}_t)\|_2^2 = \|\mathbf{R}_{\text{proj}}(\mathbf{z}_t)\|_2^2$, and the Tikhonov functional (9) can be written in terms of the projected problem,

$$P^{\zeta}(\mathbf{z}) = \|B_t\mathbf{z} - \|\tilde{\mathbf{r}}\|_2\mathbf{e}_{t+1}\|_2^2 + \zeta^2\|\mathbf{z}\|_2^2, \quad \|\mathbf{h}\|_2^2 = \|\mathbf{z}\|_2^2. \tag{15}$$

Here regularization parameter ζ replaces α while having the same role as α but for the projected case. Since the dimensions of B_t are small as compared to the dimensions of $\tilde{\tilde{G}}$, the solution of the projected problem (15) is obtained efficiently from

$$\mathbf{z}_t(\zeta) = (B_t^TB_t + \zeta^2I_t)^{-1}B_t^T\|\tilde{\mathbf{r}}\|_2\mathbf{e}_{t+1} = B_t(\zeta)\|\tilde{\mathbf{r}}\|_2\mathbf{e}_{t+1},$$

where $B_t(\zeta) = (B_t^TB_t + \zeta^2I_t)^{-1}B_t^T$ can be obtained using the SVD, see appendix A, and the update for the global solution is immediately given by $\mathbf{m}_t(\zeta) = \mathbf{m}_{\text{apr}} + W^{-1}A_t\mathbf{z}_t(\zeta)$.

The projected solution $\mathbf{z}_t(\zeta)$ depends on both the subspace size, t, and the regularization parameter, ζ. Our focus here is not on the determination of the optimal subspace size t_{opt}, rather we focus on the determination of ζ_{opt}, noting that finding t_{opt} is a topic of significant study see for example the discussion in e.g. (Renaut et al. 2015). For small t, the singular values of B_t, γ_i, approximate the largest singular values of $\tilde{\tilde{G}}$, however, for larger t the smaller singular values of B_t approximate the smallest singular values of $\tilde{\tilde{G}}$, so that there is no immediate one to one alignment of the small singular values between $\tilde{\tilde{G}}$ and B_t with increasing t. Thus, it is important to choose t such that the dominant singular values of $\tilde{\tilde{G}}$ are well approximated by those of B_t effectively capturing the dominant subspace for the solution. We will discus the effect of choosing different t on the solution. Furthermore, the regularization parameter-choice methods used in this context, also need some modification for the projected case, which is demonstrated in the next section.

Although H_{t+1} and A_t have orthonormal columns in exact arithmetic, Krylov methods lose orthogonality in finite precision. This means that after a relatively low number of iterations the vectors in H_{t+1} and A_t are no longer orthogonal and the relationship between (9) and (15) does not hold. Here

we therefore use reorthogonalization to maintain the column orthogonality, which is also important for replicating the dominant spectral properties of $\tilde{\tilde{G}}$ by B_t. We use Modified Gram Schmidt (MGS), see Hansen (2007). We summarize the steps which are needed for implementation of the projected L_1 inversion in Algorithm 2 and note that in practice one may not need to explicitly calculate $\tilde{\tilde{G}}$, rather, for the factorization it can be sufficient to be able to efficiently perform operations with $\tilde{G}$, $\tilde{G}^T$, and diagonal matrices W, as discussed in section 2 in relation to Algorithm 1.

Algorithm 2 Iterative Projected L_1 Inversion Algorithm

Input: $\mathbf{d}_{\rm obs}$, $\mathbf{m}_{\rm apr}$, G, $W_{\mathbf{d}}$, $\epsilon > 0$, $\rho_{\min}$, $\rho_{\max}$, t, $K_{\max}$

1: Calculate $W_{\rm z}$, $\tilde{G} = W_{\mathbf{d}}G$, and $\tilde{\mathbf{d}}_{\rm obs} = W_{\mathbf{d}}\mathbf{d}_{\rm obs}$
2: Initialize $\mathbf{m}^{(0)} = \mathbf{m}_{\rm apr}$, $W_{L_1}^{(1)} = I_n$, $W^{(1)} = W_{\rm z}$
3: Calculate $\tilde{\mathbf{r}}^{(1)} = \tilde{\mathbf{d}}_{\rm obs} - \tilde{G}\mathbf{m}^{(0)}$, $\tilde{\tilde{G}}^{(1)} = \tilde{G}(W^{(1)})^{-1}$, $k = 0$
4: **while** Not converged, (11) not satisfied, and $k < K_{\max}$ **do**
5: $k = k + 1$
6: Apply GKB: $\tilde{\tilde{G}}^{(k)} A_t^{(k)} = H_{t+1}^{(k)} B_t^{(k)}, \quad H_{t+1}^{(k)}\mathbf{e}_{t+1} = \tilde{\mathbf{r}}^{(k)}/\|\tilde{\mathbf{r}}^{(k)}\|_2$
7: Find the SVD: $B_t^{(k)} = U\Gamma V^T$
8: Use regularization parameter estimation to find $\zeta^{(k)}$
9: Set $\mathbf{z}_t^{(k)} = \sum_{i=1}^{t} \frac{\gamma_i^2}{\gamma_i^2 + (\zeta^{(k)})^2} \frac{\mathbf{u}_i^T(\|\tilde{\mathbf{r}}^{(k)}\|_2 \mathbf{e}_{t+1})}{\gamma_i} \mathbf{v}_i$
10: Set $\mathbf{h}_t^{(k)} = A_t^{(k)} \mathbf{z}_t^{(k)}$
11: Set $\mathbf{m}^{(k)} = \mathbf{m}^{(k-1)} + (W^{(k)})^{-1}\mathbf{h}_t^{(k)}$
12: Impose constraint conditions on $\mathbf{m}^{(k)}$ to force $\rho_{\min} \leq \mathbf{m}^{(k)} \leq \rho_{\max}$
13: Calculate the residual $\tilde{\mathbf{r}}^{(k+1)} = \tilde{\mathbf{d}}_{\rm obs} - \tilde{G}\mathbf{m}^{(k)}$
14: Set $W_{L_1}^{(k+1)} = \text{diag}\left(\left((\mathbf{m}^{(k)} - \mathbf{m}^{(k-1)})^2 + \epsilon^2\right)^{-1/4}\right)$, as in (3), and $W^{(k+1)} = W_{L_1}^{(k+1)} W_{\rm z}$
15: Calculate $\tilde{\tilde{G}}^{(k+1)} = \tilde{G}(W^{(k+1)})^{-1}$
16: **end while**

Output: Solution $\rho = \mathbf{m}^{(k)}$. $K = k$.

3 REGULARIZATION PARAMETER ESTIMATION

Now we focus on determination of the regularization parameter at each step k, supposing that the dimension of the subspace, t, is known and kept fixed during the iterations. Our previous investigations have been shown that the method of the UPRE leads to an effective estimation of the regularization parameter (Renaut et al. 2015; Vatankhah et al. 2015; Vatankhah et al. 2014b). In order to use the method for the projected problem we briefly review the derivation of the UPRE on the full problem.

3.1 Unbiased predictive risk estimator

Any method which is used to determine optimal α should minimize the error between the solution $\mathbf{h}(\alpha)$ and the exact solution $\mathbf{h}_{\text{exact}}$. Because the exact solution is unknown, an alternative error indicator, called the predictive error, is used (Vogel 2002)

$$\begin{aligned}\mathbf{P}_{\text{full}}(\mathbf{h}(\alpha)) &= \tilde{\tilde{G}}\mathbf{h}(\alpha) - \tilde{\mathbf{r}}_{\text{exact}} = \tilde{\tilde{G}}\tilde{\tilde{G}}(\alpha)\tilde{\mathbf{r}} - \tilde{\mathbf{r}}_{\text{exact}} \\ &= H(\alpha)(\tilde{\mathbf{r}}_{\text{exact}} + \tilde{\boldsymbol{\eta}}) - \tilde{\mathbf{r}}_{\text{exact}} = (H(\alpha) - I_m)\tilde{\mathbf{r}}_{\text{exact}} + H(\alpha)\tilde{\boldsymbol{\eta}} \end{aligned} \tag{16}$$

where $H(\alpha) = \tilde{\tilde{G}}\tilde{\tilde{G}}(\alpha)$ is the influence matrix. The predictive error is also not computable because $\tilde{\mathbf{r}}_{\text{exact}}$ is unknown, however, it can be estimated using the full residual (14)

$$\mathbf{R}_{\text{full}}(\mathbf{h}(\alpha)) = \tilde{\tilde{G}}\mathbf{h}(\alpha) - \tilde{\mathbf{r}} = (H(\alpha) - I_m)\tilde{\mathbf{r}} = (H(\alpha) - I_m)\tilde{\mathbf{r}}_{\text{exact}} + (H(\alpha) - I_m)\tilde{\boldsymbol{\eta}}. \tag{17}$$

For both (16) and (17), the first term on the right hand side is deterministic, whereas the second is stochastic. Applying the Trace lemma, e.g. (Vogel 2002), for both equations and using the symmetry of the influence matrix we obtain

$$E(\|\mathbf{P}_{\text{full}}(\mathbf{h}(\alpha))\|_2^2) = \|(H(\alpha) - I_m)\tilde{\mathbf{r}}_{\text{exact}}\|_2^2 + \text{trace}(H^T(\alpha)H(\alpha)), \text{ and} \tag{18}$$

$$E(\|\mathbf{R}_{\text{full}}(\mathbf{h}(\alpha))\|_2^2) = \|(H(\alpha) - I_m)\tilde{\mathbf{r}}_{\text{exact}}\|_2^2 + \text{trace}((H(\alpha) - I_m)^T(H(\alpha) - I_m)). \tag{19}$$

Here $E(\|\mathbf{P}_{\text{full}}(\mathbf{h}(\alpha))\|_2^2)/m$ is the expected value of the predictive risk (Vogel 2002). The first terms in the right hand sides of (18) and (19) are the same. Thus, by the linearity of the trace operator and with $E(\|\mathbf{R}_{\text{full}}(\mathbf{h}(\alpha))\|_2^2) \approx \|\mathbf{R}_{\text{full}}(\mathbf{h}(\alpha))\|_2^2 = \|(H(\alpha) - I_m)\tilde{\mathbf{r}}\|_2^2$, the UPRE estimator of the optimal parameter is

$$\alpha_{\text{opt}} = \arg\min_{\alpha}\{U(\alpha) := \|(H(\alpha) - I_m)\tilde{\mathbf{r}}\|_2^2 + 2\,\text{trace}(H(\alpha)) - m\}. \tag{20}$$

Typically α_{opt} is found by evaluating (20) for a range of α, for example by the SVD see appendix B, with the minimum found within that range of parameter values.

3.2 Extending the UPRE for the projected problem

For extending the UPRE parameter-choice method to a subspace, we first observe that given $\tilde{\mathbf{r}} = \tilde{\mathbf{r}}_{\text{exact}} + \tilde{\boldsymbol{\eta}}$, then $\|\tilde{\mathbf{r}}\|_2\mathbf{e}_{t+1} = H_{t+1}^T\tilde{\mathbf{r}}$ consists of a deterministic and stochastic part, $H_{t+1}^T\tilde{\mathbf{r}}_{\text{exact}} + H_{t+1}^T\tilde{\boldsymbol{\eta}}$, where for white noise vector $\tilde{\boldsymbol{\eta}}$ and column orthogonal H_{t+1}, $H_{t+1}^T\tilde{\boldsymbol{\eta}}$ is a random vector of length $t+1$ with covariance matrix I_t. Thus, from the derivation of UPRE for the full problem defined by the system matrix $\tilde{\tilde{G}}$, right hand side $\tilde{\mathbf{r}}$ and white noise vector $\tilde{\boldsymbol{\eta}}$ we immediately write down the UPRE for the projected problem with system matrix B_t, right hand side $H_{t+1}^T\tilde{\mathbf{r}}$ and white noise vector $H_{t+1}^T\tilde{\boldsymbol{\eta}}$

$$\zeta_{\text{opt}} = \arg\min_{\zeta}\{U(\zeta) := \|(B(\zeta) - I_{t+1})\|\tilde{\mathbf{r}}\|_2\mathbf{e}_{t+1}\|_2^2 + 2\,\text{trace}(B(\zeta)) - (t+1)\}. \tag{21}$$

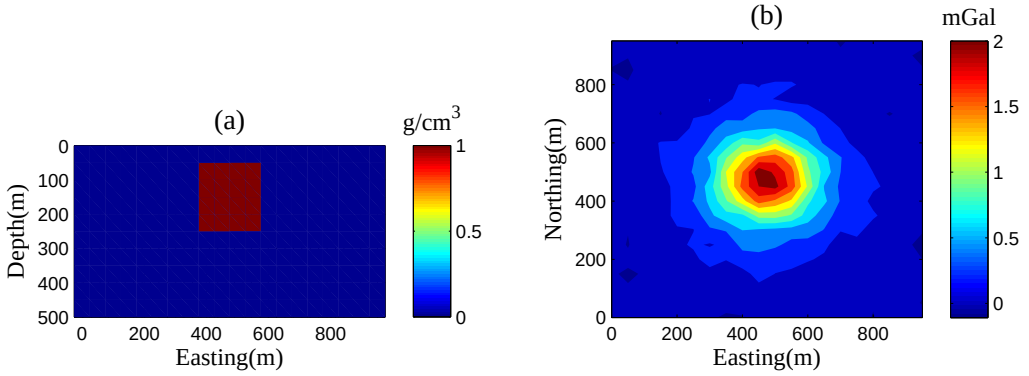

Figure 2. (a) Model of the cube on an homogeneous background. The density contrast of the cube is 1 g cm^{-3}. (b) Data due to the model and contaminated with noise $N2$.

Here $B(\zeta) = B_t B_t(\zeta)$ is the influence matrix for the subspace. As for the full problem, see appendix B, the SVD of the matrix B_t can be used to find ζ_{opt}. In section 4.1 we show that in some situations (21), as introduced in (Renaut et al. 2015), does not work well. Here, a modification is introduced that does not use the entire subspace for a given t, but rather uses a truncated spectrum from B_t for finding the regularization parameter, thus assuring that the dominant t_{trunc} singular values are appropriately regularized.

4 SYNTHETIC EXAMPLES

4.1 Model of an embedded cube

The initial goal of the presented verification with simulated data is to contrast Algorithms 1 and 2. We use a simple small-scale model that includes a cube with density contrast 1 g cm^{-3} embedded in an homogeneous background, Fig. 2(a). Simulation data on the surface, $\mathbf{d}_{\text{exact}}$, are calculated over a 20×20 regular grid with 50 m grid spacing. To add noise to the data, a zero mean Gaussian random matrix Θ of size m $\times 10$ was generated. Then, setting

$$\mathbf{d}_{\text{obs}}^c = \mathbf{d}_{\text{exact}} + (\tau_1 (\mathbf{d}_{\text{exact}})_i + \tau_2 \|\mathbf{d}_{\text{exact}}\|)\, \Theta^c, \tag{22}$$

for $c = 1 : 10$, with noise parameter pairs (τ_1, τ_2), for three choices, $N1 : (0.01, 0.001)$, $N2 : (0.02, 0.005)$ and $N3 : (0.03, 0.01)$, gives 10 noisy right-hand side vectors for 3 levels of noise. Fig. 2(b) shows noise-contaminated data for one right-hand side, here $c = 7$, and for $N2$. For the inversion the model region of depth 500 m, is discretized into $20 \times 20 \times 10 = 4000$ cells of size 50m in each dimension. The background model $\mathbf{m}_{\text{apr}} = \mathbf{0}$ and parameter $\epsilon^2 = 1e{-}9$ are chosen for the inversion. Realistic upper and lower density bounds $\rho_{\max} = 1$ g cm^{-3} and $\rho_{\min} = 0$ g cm^{-3}, are

Table 1. The inversion results obtained by inverting the data from the cube using Algorithm 1, with $\epsilon^2 = 1e{-}9$, average (standard deviation) over 10 runs.

Noise	$\alpha^{(1)}$	$\alpha^{(K)}$	$RE^{(K)}$	K
$N1$	47769.1	117.5(10.6)	0.319(0.017)	8.2(0.4)
$N2$	48623.4	56.2(8.5)	0.388(0.023)	6.1(0.6)
$N3$	48886.2	36.2(9.1)	0.454(0.030)	5.8(1.3)

specified. The iterations are terminated when, approximating (11), $\chi^2_{\text{Computed}} \leq 429$, or $k > K_{\max} = 50$.

4.2 Solution using Algorithm 1

The inversion was performed using Algorithm 1 for the 3 noise levels, and all 10 right-hand side data vectors. The final iteration K, the final regularization parameter $\alpha^{(K)}$ and the relative error of the reconstructed model

$$RE^{(K)} = \frac{\|\mathbf{m}_{\text{exact}} - \mathbf{m}^{(K)}\|_2}{\|\mathbf{m}_{\text{exact}}\|_2} \tag{23}$$

are recorded. Table 1 gives the average and standard deviation of $\alpha^{(K)}$, $RE^{(K)}$ and K over the 10 samples. It was explained by Farquharson (2004) that it is efficient if the inversion starts with a large value of the regularization parameter. This prohibits imposing excessive structure in the model at early iterations which would otherwise require more iterations to remove artificial structure. In this paper the method introduced by Vatankhah et.al. (2014a; 2015) was used to determine an initial regularization parameter, $\alpha^{(1)}$. Because the non zero singular values, σ_i of matrix $\tilde{\tilde{G}}$ are known, the initial value

$$\alpha^{(1)} = (n/m)^{3.5}(\sigma_1/\text{mean}(\sigma_{\text{i}})) \tag{24}$$

can be selected. For subsequent iterations the UPRE method is used to estimate $\alpha^{(k)}$.

To illustrate the results, Figs. 3-6 provide details for right-hand side $c = 7$ and for all noise levels. Fig. 3 shows the reconstructed models, indicating that a focused image of the subsurface is possible in all cases using Algorithm 1. The constructed models have sharp and distinct interfaces with the embedded medium. The progression of the data misfit $\Phi(\mathbf{m})$, the regularization term $S(\mathbf{m})$ and regularization parameter $\alpha^{(k)}$ with iteration k are presented in Fig. 4. $\Phi(\mathbf{m})$ is initially large and decays quickly in the first few steps, but the decay rate decreases dramatically as k increases. Fig. 5 shows the progression of the relative error, (23), as a function of k. In all cases there is a dramatic decrease in the relative error for small k, after which the error decreases slowly. The UPRE functional for iteration $k = 4$ is shown in Fig. 6. Clearly, for all cases the curves have a nicely defined

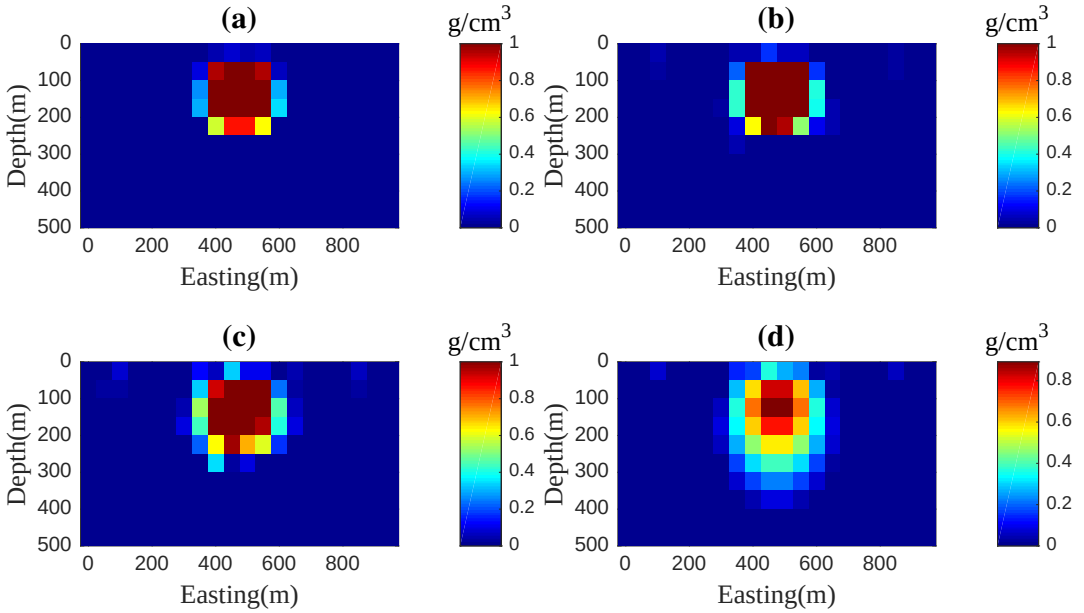

Figure 3. The reconstructed model obtained by inverting the noise-contaminated right-hand side with $c = 7$ using Algorithm 1 for noise cases (a) $N1$; (b) $N2$; (c) $N3$ with $\epsilon^2 = 1e{-}9$ and (d) $N2$ when $\epsilon^2 = 0.5$.

minimum, which is important in the determination of the regularization parameter. We return to this when considering the projected case.

To determine the dependence of Algorithm 1 on other values of ϵ^2, we examined the results using right-hand side data for $c = 7$ for noise $N2$ with $\epsilon^2 = 0.5$ and $\epsilon^2 = 1e{-}15$ with all other parameters chosen as before. For $\epsilon^2 = 1e{-}15$ the results are very close to those obtained with $\epsilon^2 = 1e{-}9$, and are not presented here. For $\epsilon^2 = 0.5$ the results are significantly different. Fig. 3(d) shows the reconstructed model, indicating a smeared-out and fuzzy image of the original model. The maximum of the obtained density is about 0.85 g cm^{-3}, 85% of the imposed $\rho_{\max}$. The progression of the data misfit, the regularization term and regularization parameter are presented in Fig. 4(d), while the relative error functional and UPRE curve at iteration 4 are shown in Fig. 5(d) and Fig. 6(d), respectively. Clearly more iterations are needed to terminate the algorithm, $K = 31$, and at the final iteration $\alpha^{(31)} = 1619.2$ and $RE^{(K)} = 0.563$ respectively, larger than their counterparts in the case $\epsilon^2 = 1e{-}9$.

4.3 Solution using Algorithm 2

Algorithm 2 is used to reconstruct the model for 4 different values of t, $t = 3$, 100, 200 and 400, in order to examine the impact of the size of the projected subspace on the solution and the estimated parameter ζ. The results for $t < m$, are given in Table 2. Here, in order to compare the algorithms, the initial regularization parameter, $\zeta^{(1)}$, is set to the value that would be used on the full space. Generally, for small t the estimated regularization parameter is less than the counterpart obtained for the full case

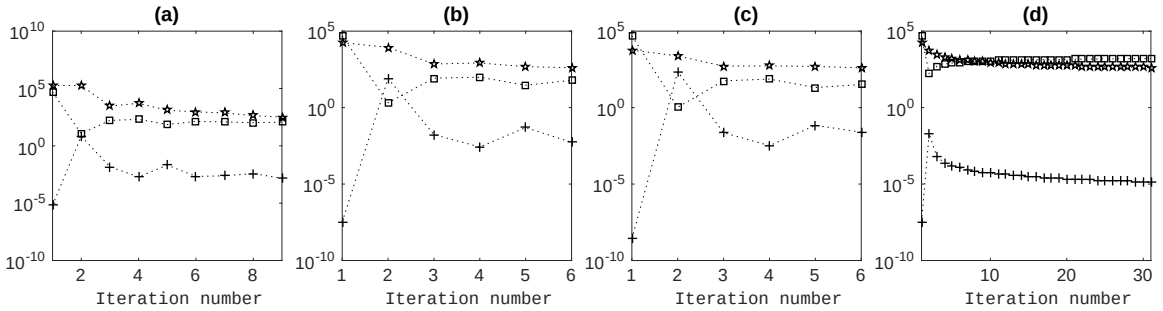

Figure 4. Inverting the noise-contaminated right-hand side with $c = 7$ using Algorithm 1. The progression of the data misfit, $\star$, the regularization term, $+$, and the regularization parameter, $\square$, with iteration k for noise cases (a) $N1$; (b) $N2$; (c) $N3$ with $\epsilon^2 = 1e{-}9$ and (d) $N2$ when $\epsilon^2 = 0.5$.

for the specific noise level. Comparing Tables 1 and 2 it is clear that with increasing t, the estimated ζ increases, reaching $\alpha^{(K)}$ of the full space when $t = m$. For $t = 3$, the algorithm is computationally very fast and the relative error of the reconstructed model is acceptable, but still larger than that obtained using the full model. As t becomes greater than 3, and approaches $t = 200$, the results are not satisfactory. For a sample case, $t = 100$, the results are presented in Table 2. The relative error is very large and the reconstructed model is generally not acceptable. Although the results with the least noise are acceptable, they are still worse than the results obtained with the other selected choices for t. In this case, $t = 100$, and for high noise levels, the algorithm usually terminates when it reaches $k = K_{\max} = 50$, indicating that the solution does not satisfy the noise level constraint (11). For $t = 200$ the results are again acceptable, although less satisfactory than the results obtained with the full space. With increasing t the results improve, until for $t = m = 400$ the results, not given here, reproduce, as expected, those obtained with Algorithm 1.

To illustrate the results, we show the reconstructed models using Algorithm 2 with different t and

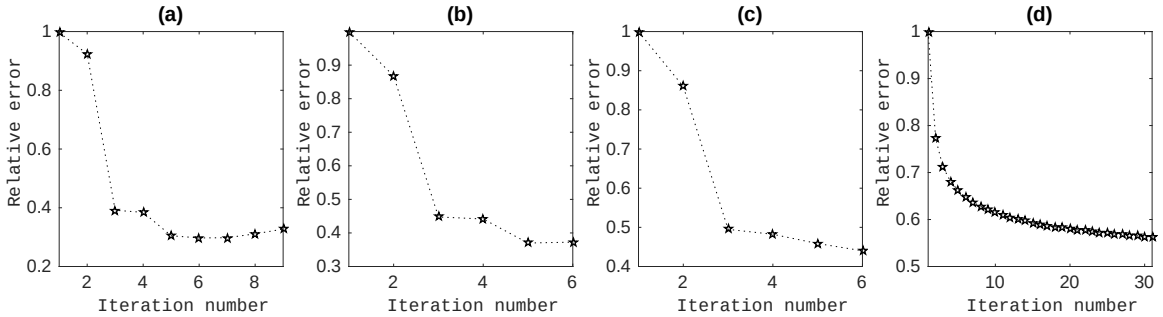

Figure 5. Inverting the noise-contaminated right-hand side with $c = 7$ using Algorithm 1. The progression of the relative error at each iteration for noise cases (a) $N1$; (b) $N2$; (c) $N3$ with $\epsilon^2 = 1e{-}9$ and (d) $N2$ when $\epsilon^2 = 0.5$.

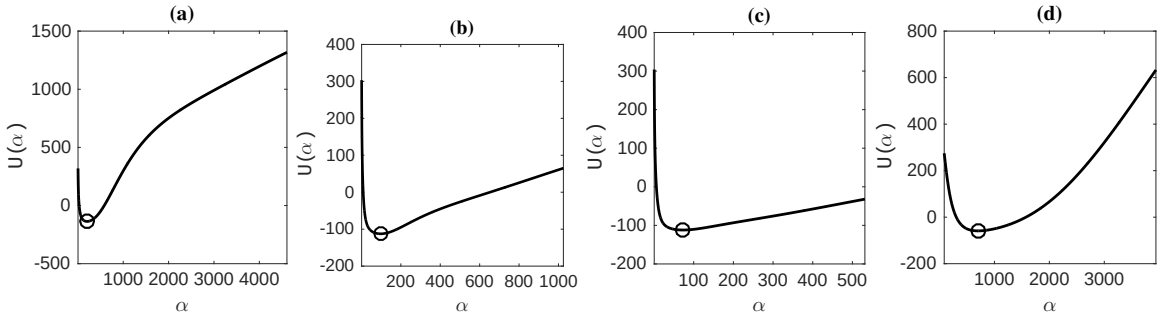

Figure 6. Inverting the noise-contaminated right-hand side with $c = 7$ using Algorithm 1. The UPRE functional at iteration 4 for noise cases (a) $N1$; (b) $N2$; (c) $N3$ with $\epsilon^2 = 1e{-}9$ and (d) $N2$ when $\epsilon^2 = 0.5$.

for right-hand side $c = 7$ for noise $N2$, Fig. 7. As illustrated, the reconstructed models for $t = 3$, 200 and 400 are acceptable, while for $t = 100$ the results are completely wrong. For some right-hand sides c with $t = 100$, the reconstructed models may be much worse than that shown in Fig. 7(b). The progression of the data misfit, the regularization term and the regularization parameter with iteration k are presented in Fig. 8, while $RE^{(K)}$ is shown in Fig. 9. For $t = 100$ and for high noise levels, usually the estimated value for $\zeta^{(k)}$ using (21) for $1 < k < K$ is small, corresponding to under regularization and yielding a large error in the solution. To understand why the UPRE leads to under regularization we illustrate the UPRE curves for iteration $k = 4$ in Fig. 10. It is immediate that when using small t, $U(\zeta)$ may not have a unique minimum, and thus the algorithm may find a minimum at a small regularization parameter which leads to under regularization of the dominant, and more accurate, terms in the expansion. This can cause problems for moderate t, $t < 200$. On the other hand, as t increases, e.g. for $t = 200$ and 400, it appears that there is a unique minimum of $U(\zeta)$ and the regularization parameter found is appropriate. Unfortunately, this situation creates a conflict with the need to use $t \ll m$ for large scale problems.

Table 2. The inversion results obtained by inverting the data from the cube using Algorithm 2, with $\epsilon^2 = 1e{-}9$, and $\zeta^{(1)} = \alpha^{(1)}$ for the specific noise level as given in Table 1. In each case the average (standard deviation) over 10 runs. The rows corresponding to noise cases $N1$, $N2$ and $N3$, resp.

	t=3		t=100			t=200		
$\zeta^{(K)}$	$RE^{(K)}$	K	$\zeta^{(K)}$	$RE^{(K)}$	K	$\zeta^{(K)}$	$RE^{(K)}$	K
75.5(2.9)	.427(.037)	13.5(0.5)	98.9(12.0)	.452(.043)	10.0(0.7)	102.2(11.3)	.330(.019)	8.8(0.4)
46.7(14.2)	.472(.041)	7.8(0.6)	42.8(10.4)	1.009(.184)	28.1(10.9)	43.8(7.0)	.429(.053)	6.7(0.8)
25.6(4.7)	.493(.03)	6.1(0.7)	8.4(13.3)	1.118(.108)	42.6(15.6)	27.2(6.3)	.463(.036)	5.5(0.5)

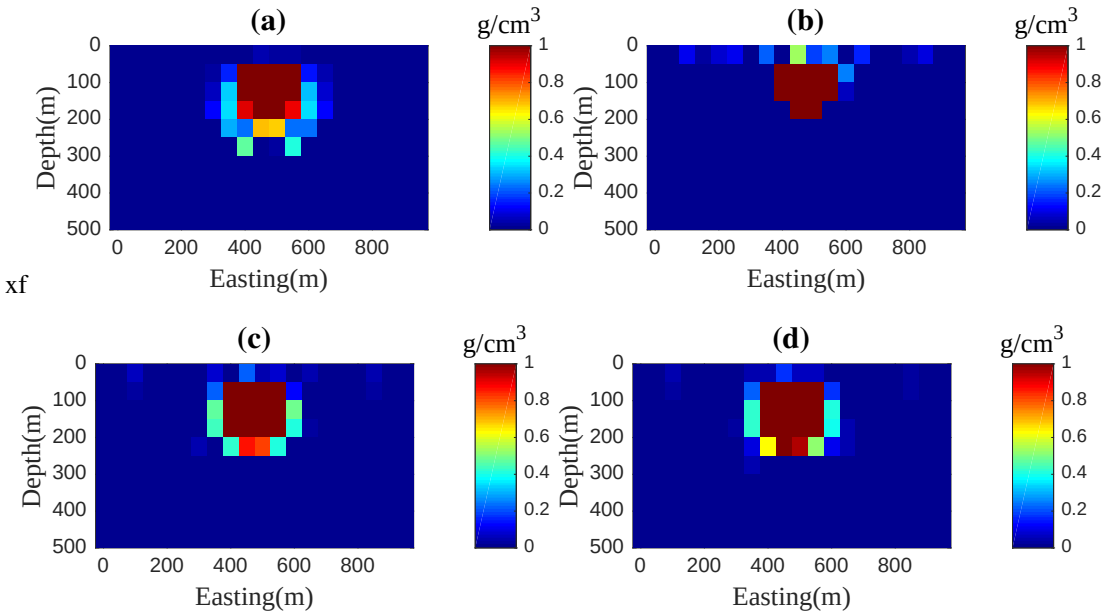

Figure 7. The reconstructed model obtained by inverting the noise-contaminated right-hand side with $c = 7$ for noise $N2$ using Algorithm 2 with $\epsilon^2 = 1e{-}9$. (a) $t = 3$; (b) $t = 100$; (c) $t = 200$; and (d) $t = 400$.

4.4 Extending the projected UPRE by spectrum truncation

To determine the reason for the difficulty with using $U(\zeta)$ to find an optimal ζ for moderate t, we illustrate the singular values for B_t and $\tilde{\tilde{G}}$ in Fig. 11 for the chosen choices of t for iteration 4 and for the case with $t = 100$ the singular values at iterations 1, 3, 5 and the final iteration 14. It can be seen that for moderate t, we have $\gamma_i \approx \sigma_i$ only for $i = 1 : t^*$ for some $t^* < t$, where as seen from Figs. 11(e)-11(h), t^* is approximately preserved with the iterative steps. Now, for $i > t^*$, $\gamma_i << \sigma_i$, as B_t reflects the overall condition of the problem. This generates regularization parameters which are determined by the smallest γ_i, rather than the dominant terms. Suppose, on the other hand, that we use

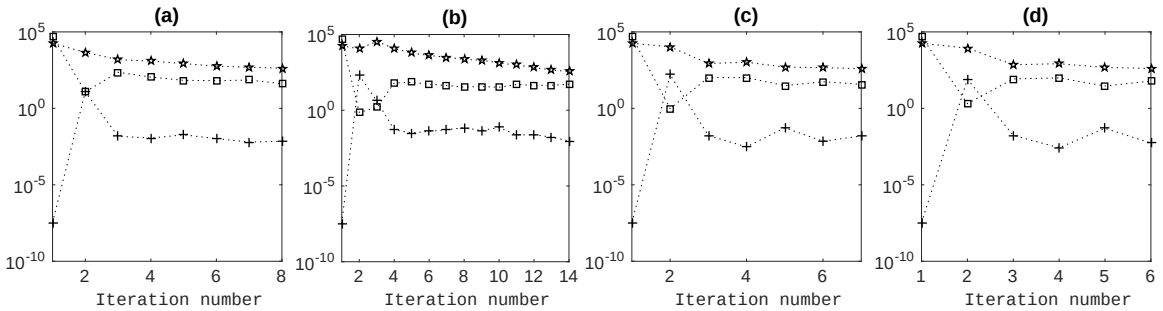

Figure 8. Inverting the noise-contaminated right-hand side with $c = 7$ for noise $N2$ using Algorithm 2 with $\epsilon^2 = 1e{-}9$. The progression of the data misfit, $\star$, the regularization term, $+$, and the regularization parameter, $\square$, with iteration k, for (a) $t = 3$; (b) $t = 100$; (c) $t = 200$; and (d) $t = 400$.

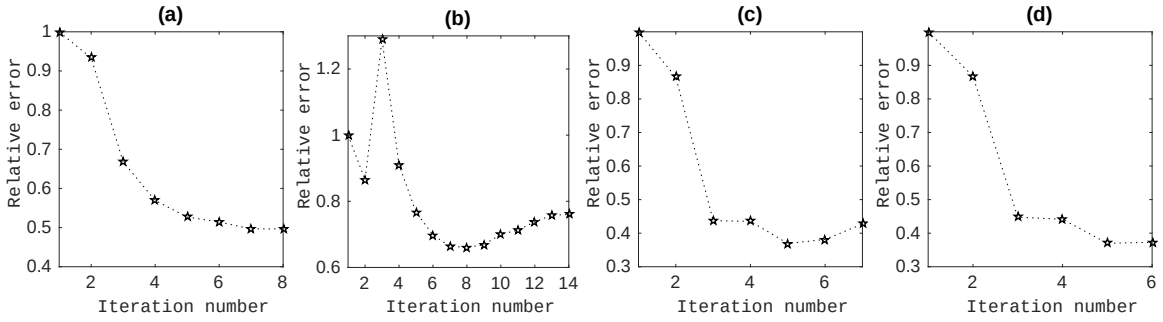

Figure 9. Inverting the noise-contaminated right-hand side with $c = 7$ for noise $N2$ using Algorithm 2 with $\epsilon^2 = 1e{-}9$. The progression of the relative error at each iteration for (a) $t = 3$; (b) $t = 100$; (c) $t = 200$; and (d) $t = 400$.

t steps of the GKB on matrix $\tilde{\tilde{G}}$ to obtain B_t, but use $t_{\rm trunc} = \omega\, t$, $\omega < 1$, singular values of B_t in estimating both ζ and z_t, in steps 8 and 9 of Algorithm 2. Our examinations, see for example Fig. 11, suggest taking $\omega \approx 0.8$, with this choice consistent across all iterations. With this choice the smallest singular values of B_t are ignored in estimating ζ and z_t.

We denote the approach, in which we replace steps 8 and 9 in Algorithm 2 with estimates using $t_{\rm trunc}$, truncated UPRE (TUPRE). We comment that the approach may work equally well for alternative regularization techniques, but this is not a topic of the current investigation, as is a detailed investigation for the choice of ω. For example, our investigations show that ω may be estimated at the first iteration by examining the singular values for $B_{\hat{t}}$ where $\hat{t} > t$, say $\hat{t} = 1.1t$ and comparing how many of the singular values for B_t are close to the first t of these for $B_{\hat{t}}$, even though for this first iteration $\zeta^{(1)}$ is set large as in the estimation of $\alpha^{(1)}$, using (24), (Vatankhah et al. 2014a; Vatankhah et al. 2015). If the relative change in the spectral value is say greater than 10% for a given i then this suggests using $t_{\rm trunc} = i$, and generally corresponds to our choice $\omega \approx .8$. Furthermore, we note this is not a standard filtered truncated SVD for the solution, rather the truncation here is determined for

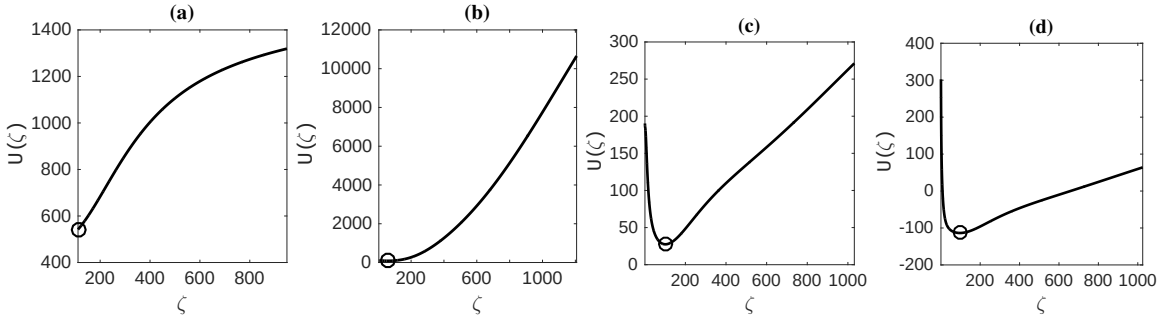

Figure 10. Inverting the noise-contaminated right-hand side with $c = 7$ for noise $N2$ using Algorithm 2 with $\epsilon^2 = 1e{-}9$. The UPRE functional at iteration 4 for (a) $t = 3$; (b) $t = 100$; (c) $t = 200$; and (d) $t = 400$.

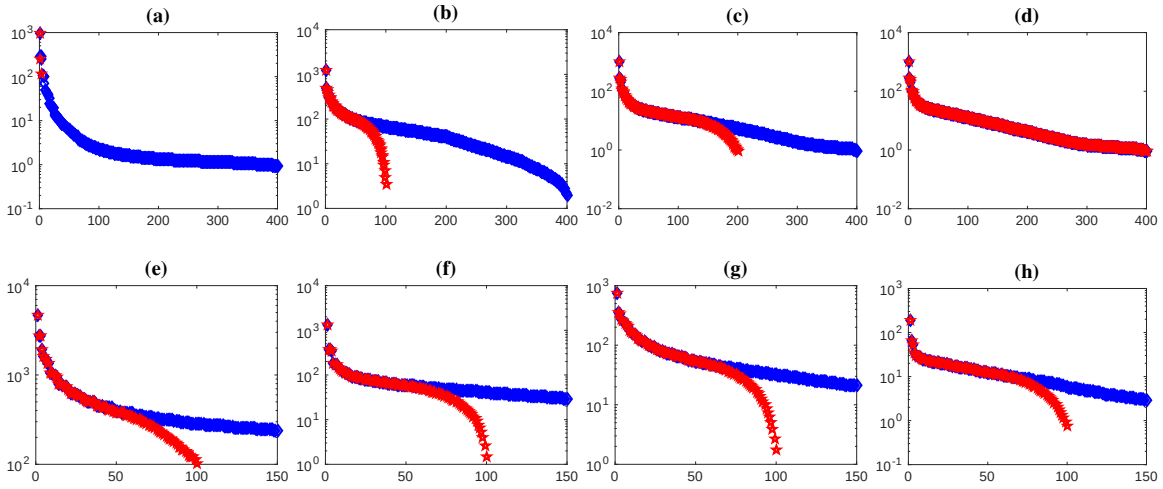

Figure 11. The singular values of $\tilde{\tilde{G}}$, blue $\diamond$, and B_t, red $\star$, at iteration 4 using Algorithm 2 with $\epsilon^2 = 1e{-}9$ for the noise-contaminated right-hand side with $c = 7$ and noise $N2$. (a) $t = 3$; (b) $t = 100$; (c) $t = 200$ and $t = 400$, for plots 11(a)-11(d). In 11(e)-11(h) the singular values of B_t for $t = 100$ and the first 150 singular values of $\tilde{\tilde{G}}$, for iterations 1, 3, 5 and the final iteration 14.

the given projected problem and is based on the accuracy of the largest possible projected subspace for a given t, which is a fraction of the anticipated subspace size t. To show the efficiency of TUPRE, we run the inversion algorithm for case $t = 100$ for which the original results are not realistic. The results using TUPRE are given in Table 3 for noise $N1$, $N2$ and $N3$, and illustrated, for right-hand side $c = 7$ for noise $N2$, in Fig. 12. Fig. 12(c) shows the existence of a well-defined minimum for $U(\zeta)$ at iteration $k = 4$, as compared to Fig. 10(b), although this is not preserved over all iterations. Reconstructed models using TUPRE for $t = 10$, 20, 30 and 40 are illustrated in Fig. 13. The results indicate that the use of TUPRE yields acceptable solutions for these moderate choices of t. Although these results show that small t can be used in the method, we suggest that $t > m/20$ is a suitable choice for this application. For high noise levels using $\omega \approx 0.7$ may improve the results. Here we use $\omega \approx 0.8$ for all cases.

Table 3. The inversion results obtained by inverting the data from the cube using Algorithm 2, with $\epsilon^2 = 1e{-}9$, using TUPRE with $t = 100$, and $\zeta^{(1)} = \alpha^{(1)}$ for the specific noise level as given in Table 1. In each case the average (standard deviation) over 10 runs.

Noise	$\zeta^{(K)}$	$RE^{(K)}$	K
$N1$	148.0(12.5)	0.299(0.010)	6.7(0.7)
$N2$	62.6(4.7)	0.384(0.035)	6.4(0.5)
$N3$	33.2(4.7)	0.445(0.034)	6.7(1.1)

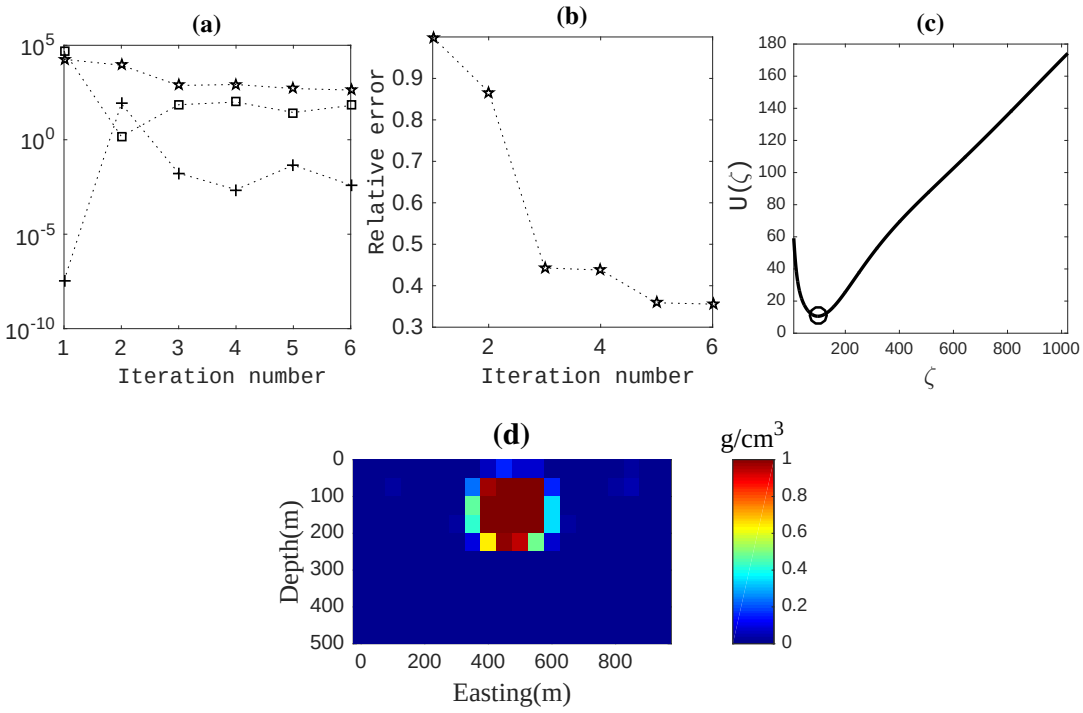

Figure 12. Results for right-hand side $c = 7$ for noise $N2$ using Algorithm 2, with $\epsilon^2 = 1e{-}9$ using TUPRE when $t = 100$ is chosen; (a) The progression of the data misfit, $\star$, the regularization term, $+$, and the regularization parameter, $\square$, with iteration k; (b) The progression of the relative error at each iteration; (c) The TUPRE functional at iteration 4; and (d) The reconstructed model.

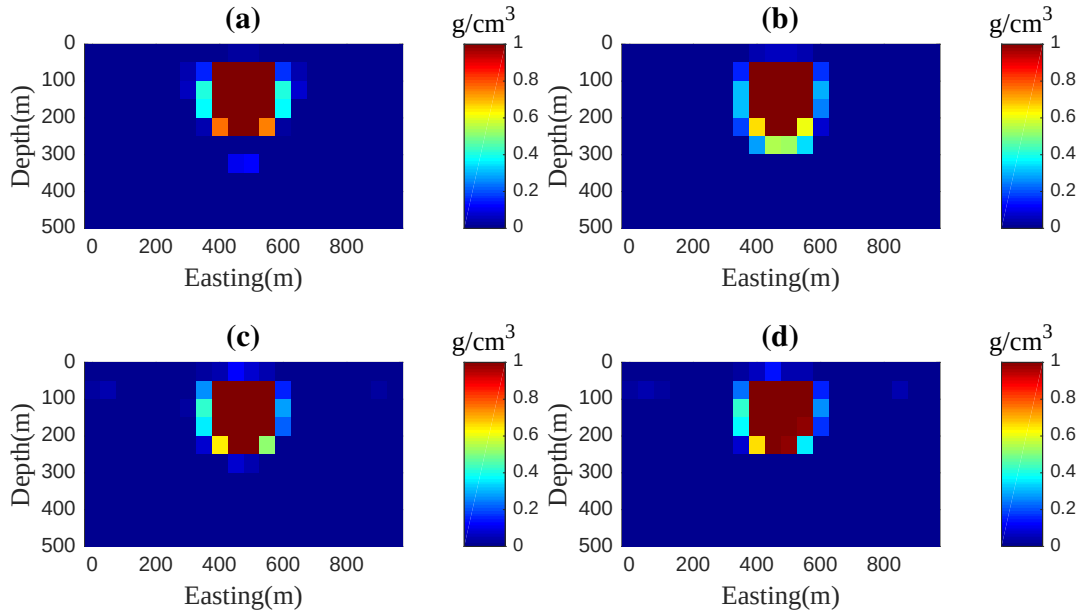

Figure 13. The reconstructed model by inverting noise-contaminated for right-hand side $c = 7$ for noise $N2$ using Algorithm 2, with $\epsilon^2 = 1e{-}9$, using TUPRE. (a) $t = 10$; (b) $t = 20$; (c) $t = 30$ and (d) $t = 40$.

4.5 Model of multiple embedded bodies

A model consisting of four bodies with various geometries, sizes, depths and densities is used to verify the ability and limitations of Algorithm 2 implemented with TUPRE for the recovery of large-scale and more complex structures. Fig. 14(a) shows a perspective view of this model. The densities of the dipping dike, anomaly A, and cube B are 0.8 g cm^{-3}, and 1 g cm^{-3} for cubes C and D. Fig. 15 shows four plane-sections of the model. The surface gravity data are calculated on a 60×60 grid with 100 m spacing, for a data vector of length 3600. Noise is added to the exact data vector as in (22) with $(\tau_1, \tau_2) = (.02, .002)$. Fig. 14(b) shows the noise-contaminated data.

The subsurface extends to depth 1000 m with cells of size 100 m in each dimension yielding the unknown model parameters to be found on $60 \times 60 \times 10 = 36000$ cells. The inversion assumes $\mathbf{m}_{\rm apr} = \mathbf{0}$, $\epsilon^2 = 1e{-}9$ and imposes density bounds $\rho_{\rm min} = 0$ g cm^{-3} and $\rho_{\rm max} = 1$ g cm^{-3}. The iterations are terminated when, approximating (11), $\chi^2_{\rm Computed} \leq 3685$, or $k > K_{\rm max} = 100$. The inversion is performed using Algorithm 2 but with the TUPRE solution methods for steps 8 amd 9. The initial regularization parameter is $\zeta^{(1)} = (n/m)^{3.5}(\gamma_1/{\rm mean}(\gamma_{\rm i}))$, for γ_i, $i = 1 : t$.

Fig. 16 shows the resulting model for the inversion, when $t = 200$ is chosen. The progression of the data misfit, the regularization term and the regularization parameter with iteration k, the TUPRE functional at the final iteration, and the progression of the relative error at each iteration are presented in Fig. 17. Convergence is reached after 11 iterations, and $\zeta^{(11)} = 50.3$. As illustrated, the horizontal borders of the bodies are recovered and the depths to the top are close to those of the original model. At the intermediate depth, the shapes of the anomalies are reconstructed well, while deeper in the subsurface additional structures appear. The reconstruction of the dipping dike is acceptable but does not completely match the original model. Using the incorrect upper density bounds for anomalies A and B, impacts the resulting model. For anomaly B the maximum density is obtained 1 g cm^{-3}, although in deeper parts it is close to the true value 0.8 g cm^{-3}. Algorithm 2 is very fast, requiring only a few minutes, dependent on the choice of t.

4.6 Comparison of L_1 and MS stabilizers

To compare with results obtained using the MS stabilizer, we implement Algorithm 2 with step 14 for finding W_{L_1} replaced by calculation of W_ϵ as in (2). Equivalently we replace $p = 1$ by $p = 0$ in (7). We use $\epsilon^2 = 1e{-}5$. The results are presented in Figs. 18 and 19. Although the MS solution is more focused, the convergence of the solution to an acceptable error level takes more iterations. Here the algorithm terminates at $k = K_{\rm max} = K_{100}$, indicating that the noise level condition (11) was not achieved. We note that, although, smaller values of ϵ provide a more focused image, the solution is less stable. For example, using $\epsilon^2 = 1e^{-9}$ the reconstructed model is more focused but is less stable.

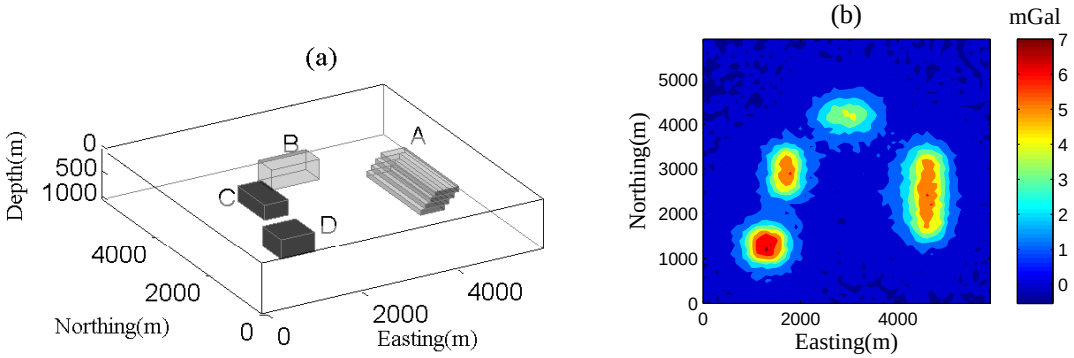

Figure 14. (a) The perspective view of the model. Four different bodies embedded in an homogeneous background. Densities of A and B are 0.8 g cm^{-3} and C and D are 1 g cm^{-3}; (b) The noise contaminated gravity anomaly due to the model.

In contrast, as indicated in Section 4.1, this is not an important issue for the L_1 stabilizer which is less sensitive to the choice of ϵ. Although there are advantages and disadvantages to each algorithm, neither is superior, it is clear that the L_1 stabilizer offers an acceptable and efficient alternative to the standard MS approach.

5 REAL DATA

To illustrate the relevance of the approach for practical data we investigate the reconstruction of gravity data acquired over a hematite mine. The survey area is near the village of Gheshmeh Gaz, Kerman province, in the southeast of Iran. The gravity survey was performed by the Gravity Branch of the Institute of Geophysics, at the University of Tehran. In this area mostly pyroclastic sediments were formed in the upper Cambrian and Devonian. The Devonian outcrops have been formed mostly from dolomitic limestone but the pyroclastic sediments of the Cambrian have been formed from rhyolite, tuff and rhyodacite, and iron oxide (Hematite) can be seen in the outcrops. Data were measured at 750 stations spaced about 10 m along the profile with 30 m between profiles. The measurements have been corrected for effects caused by variation in elevation, latitude and topography to yield the Bouguer gravity anomaly. The residual gravity anomaly has been computed using a polynomial fitting method, which was sampled every 10 m, providing a grid with $41 \times 73 = 2993$ gravity measurements. To suppress effects of noise the residual anomaly is upward-continued to a height of 2.5 m. The resulting anomaly is shown in Fig.20. Several major areas of high gravity are observed in the map, and are labeled as positions 1, 2, 3 and 4. In the western part of the region, the extension of anomalies 1 and 3 is cut off at the boundary. At the moment, no gravity data beyond the western boundary is available. We suppose each datum has an error with standard deviation $(0.02(\mathbf{d}_{\text{obs}})_i + 0.003\|\mathbf{d}_{\text{obs}}\|)$.

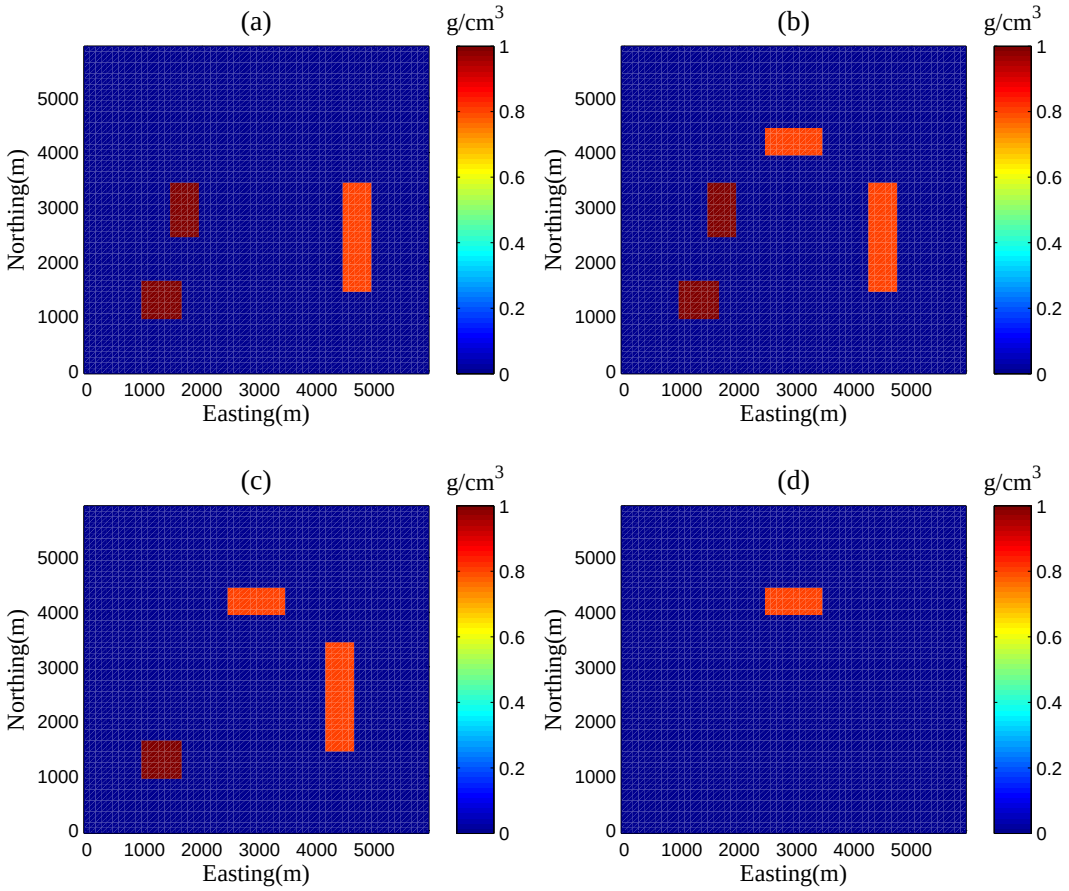

Figure 15. The original model is displayed in four plane-sections. The depths of the sections are: (a) $Z = 100$ m; (b) $Z = 300$ m; (c) $Z = 400$ m and (d) $Z = 500$ m.

For the data inversion we use a model with cells of width 10 m in the eastern and northern directions. In the depth dimension the first four layers of cells have a thickness of 5 m, while the subsequent layers increase gradually to 10 m. The maximum depth of the model is 100 m. This yields a model with the z-coordinates: $0 : 5 : 20$, 26, 33, 41, $50 : 10 : 100$. The original model is then padded in the horizontal directions with three cells with dimensions that are the same as in the original model. A mesh with $47 \times 79 \times 13 = 48269$ cells results. Based on geological information, the background density is taken to be 2.85 g cm^{-3} and density limits $\rho_{\min} = 2.5$ g cm^{-3} and $\rho_{\max} = 4$ g cm^{-3} are imposed. The TUPRE with $t = 200$ and the L_1 stabilizer with $\epsilon^2 = 1.e{-}9$ is used for the inversion by algorithm 2.

The algorithm terminates after 19 iterations. The progression of the data misfit, the regularization term and the regularization parameter with iteration k, the TUPRE functional at the final iteration, and the gravity response of the reconstructed model are shown in Fig. 21. The predicted data provide a good fit to the observed data, see Fig. 21(c). Cross-sections of the recovered model are shown in

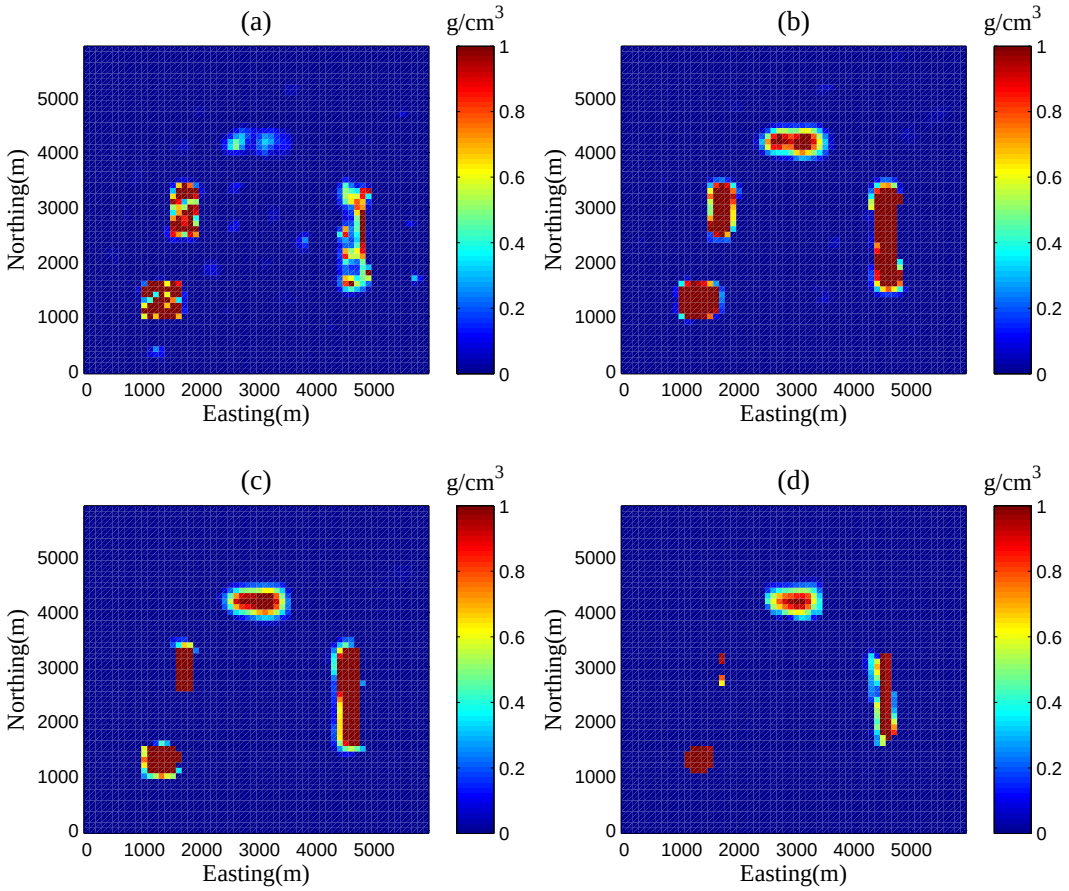

Figure 16. For the data in Fig. 14(b): The reconstructed model using Algorithm 2 with $t = 200$ and the L_1 stabilizer with $\epsilon^2 = 1.e{-}9$. The depths of the sections are: (a) $Z = 100$ m; (b) $Z = 300$ m; (c) $Z = 400$ m and (d) $Z = 500$ m.

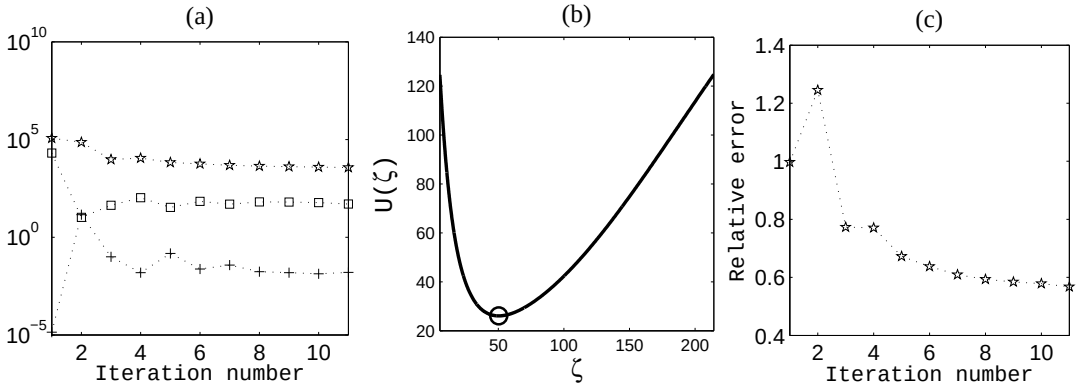

Figure 17. For the data in Fig. 14(b) using Algorithm 2 with $t = 200$ and the L_1 stabilizer with $\epsilon^2 = 1.e{-}9$. (a) The progression of the data misfit, $\star$, the regularization term, $+$, and the regularization parameter, $\square$, with iteration k; (b) The TUPRE functional at iteration 11; and (c) The progression of the relative error at each iteration.

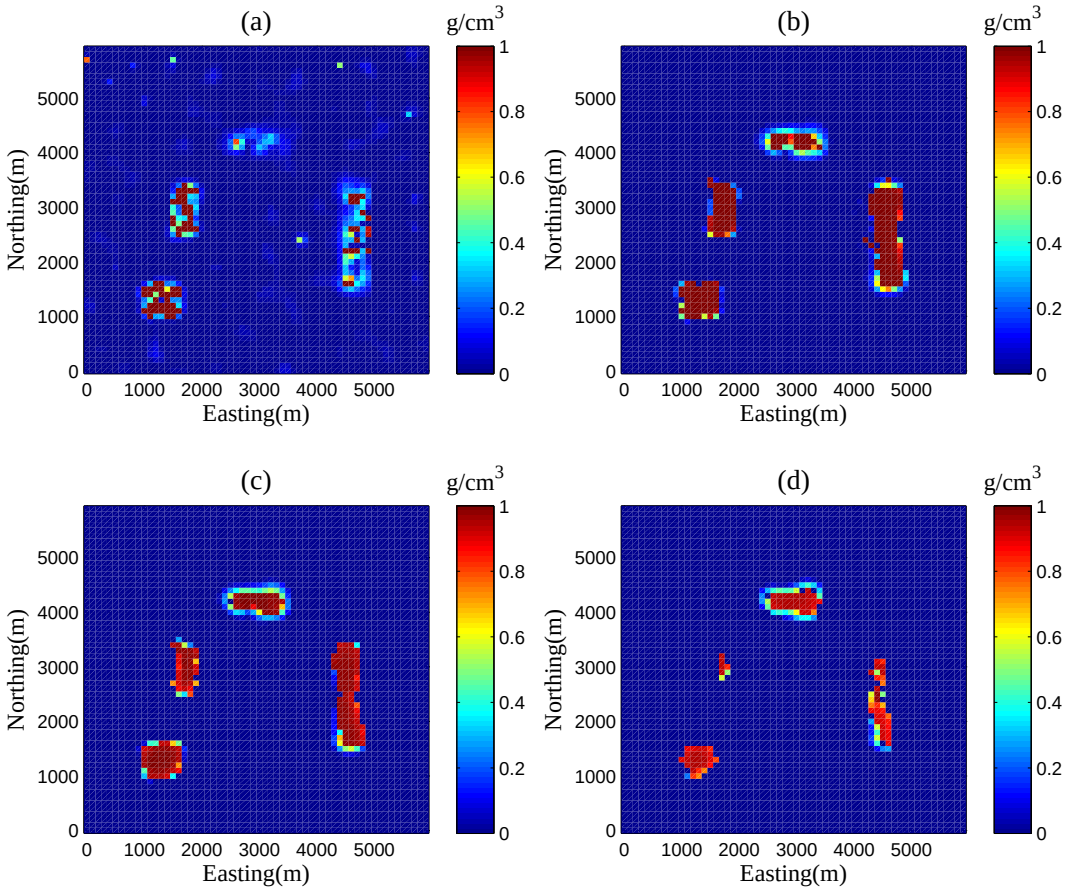

Figure 18. For the data in Fig. 14(b) using Algorithm 2 with $t = 200$ and the MS stabilizer with $\epsilon^2 = 1e-5$. The depths of the sections are: (a) $Z = 100$ m; (b) $Z = 300$ m; (c) $Z = 400$ m and (d) $Z = 500$ m.

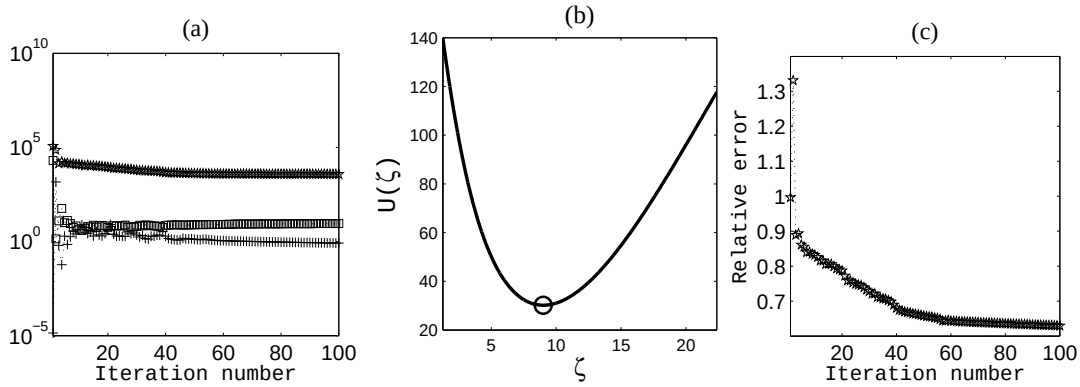

Figure 19. For the data in Fig. 14(b) using Algorithm 2 with $t = 200$ and the MS stabilizer with $\epsilon^2 = 1e-5$. (a) The progression of the data misfit, $\star$, the regularization term, $+$, and the regularization parameter, $\square$, with iteration k; (b) The TUPRE functional at iteration 100; and (c) The progression of the relative error at each iteration.

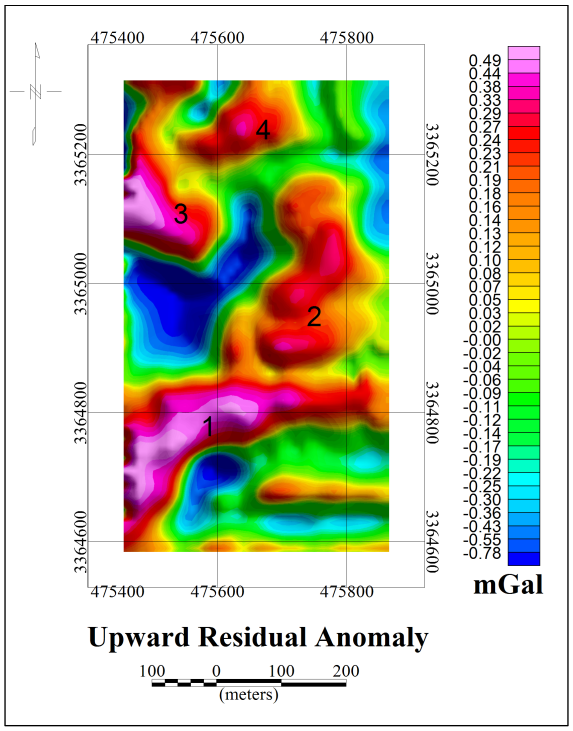

Figure 20. Upward Residual Anomaly.

Fig. 22. These are cross-sections in the northern dimension at north=100 m, 210 m, 400 m, 500 m, 650 m, and in the eastern dimension at east=20 m, 100 m, 200 m, 280 m, 350 m, in Figs.22(a)-22(b), respectively.

From Fig. 22, three major density sources are observed beneath anomalies 1, 2 and 3. The source under anomaly 4 and some small sources in the eastern part of the area are not comparable with these major sources. The maximum extension of source 1 in the west-east and south-north directions are approximately 250 m and 200 m, respectively. The depth to the surface varies between 5-10 m in the east to 20 m in the west. In the southwest, the source has a dipping form and extends to a maximum 70 m depth. Source 2 is approximately of horizontal dimnesions 100 m by 100 m, and extends from 15-25 m to 50-60 m in depth. Source 3 has a maximum extension of approximately 150 m in the west-east dimension and approximately 100 m in the south-north dimension The source is quite close to the surface, approximately at depth 5-10 m, and extends to an approximate maximum of 50 m. There are currently no data that confirm or reject the inversion results, however, based on the synthetic examples we can suppose that the inversion has yielded information that is close to the true subsurface model.

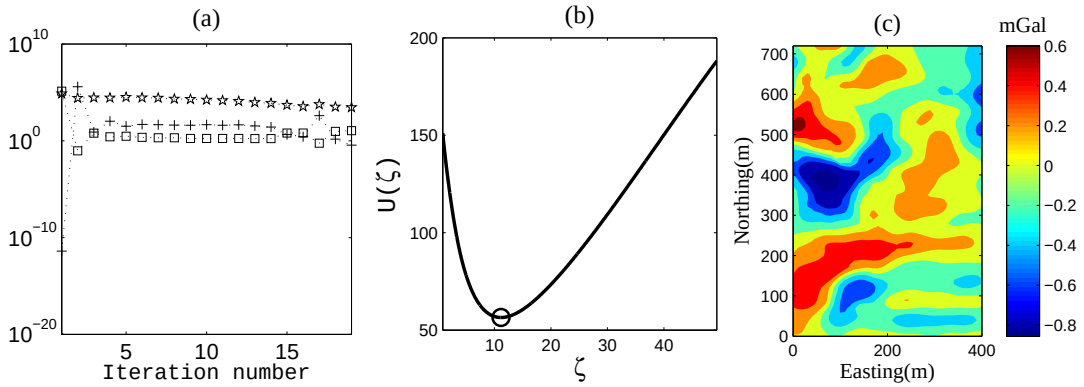

Figure 21. For the real data inversion for the data in Fig. 20: (a) The progression of the data misfit, $\star$, the regularization term, $+$, and the regularization parameter, $\square$, with iteration k; (b) The TUPRE functional at iteration 19; and (c) The gravity response of the reconstructed model.

6 CONCLUSION

We have developed an algorithm for sparse inversion of gravity data using an L_1 norm stabilizer. The algorithm is developed for both small and large scale problems. Our results show that the large scale problem can be efficiently and effectively inverted using the GKB projection with regularization applied on the projected space. We demonstrated that for estimating the regularization parameter on the subspace, a new approach based on the truncation of the projected spectrum in conjunction with the method of unbiased predictive risk should be applied. The new method, here denoted as TUPRE, gives results using the projected subspace algorithm which are comparable with those obtained for the full space, while just requiring a small number of Golub-Kahan iterations. Then, a fast and practical algorithm for the large-scale inversion of gravity data was obtained. Numerical simulations support the use of the algorithm. Finally, the algorithm was used on gravity data from a hematite mine in Iran

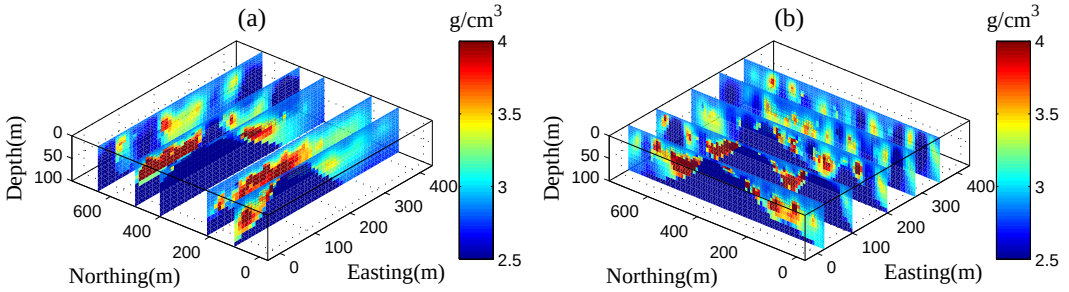

Figure 22. For the data in Fig. 20: The reconstructed model using Algorithm 2 with $t = 200$ and the L_1 stabilizer with $\epsilon^2 = 1.e{-}9$. (a) west-east cross-sections and (b) north-south cross-sections.

and the reconstructed model was shown. Future work will look further at the algorithm for other data sets, and additional justification mathematically of the truncated UPRE algorithm,

ACKNOWLEDGMENTS

Rosemary Renaut acknowledges the support of NSF grant DMS 1418377: "Novel Regularization for Joint Inversion of Nonlinear Problems".

REFERENCES

Ajo-Franklin, J. B., Minsley, B. J. & Daley, T. M., 2007. Applying compactness constraints to differential traveltime tomography, *Geophysics*, **72(4)**, R67-R75.

Boulanger, O. & Chouteau, M., 2001. Constraint in 3D gravity inversion, *Geophysical prospecting*, **49**, 265-280.

Bruckstein, A. M., Donoho, D. L. & Elad, M., 2009. From Sparse Solutions of Systems of Equations to Sparse Modeling of Signals and Images, *SIAM Rev.*, **51(1)**, 34–81.

Chung, J., Nagy, J. & O'Leary, D. P., 2008. A weighted GCV method for Lanczos hybrid regularization *ETNA*, **28**, 149-167.

Farquharson, C. G., 2008. Constructing piecwise-constant models in multidimensional minimum-structure inversions, *Geophysics*, **73(1)**, K1-K9.

Farquharson, C. G. & Oldenburg, D. W., 1998. Nonlinear inversion using general measure of data misfit and model structure, *Geophys.J.Int.*, **134**, 213-227.

Farquharson, C. G. & Oldenburg, D. W., 2004. A comparison of Automatic techniques for estimating the regularization parameter in non-linear inverse problems, *Geophys.J.Int.*, **156**, 411-425.

Gazzola, S. & Nagy, J. G., 2014. Generalized Arnoldi-Tikhonov method for sparse reconstruction, *SIAM J. Sci. Comput.*, **36(2)**, B225-B247.

Golub, G. H., Heath, M. & Wahba, G., 1979. Generalized Cross Validation as a method for choosing a good ridge parameter, *Technometrics*, **21 (2)**, 215-223.

Golub, G. H. & van Loan, C., 1996. *Matrix Computations*, (John Hopkins Press Baltimore) 3rd ed.

Hansen, P. C., 1992. Analysis of discrete ill-posed problems by means of the L-curve, *SIAM Review*, **34 (4)**, 561-580.

Hansen, P. C., 2007. *Regularization Tools: A Matlab Package for Analysis and Solution of Discrete Ill-Posed Problems Version* 4.1 *for Matlab* 7.3 , Numerical Algorithms, **46**, 189-194.

Kilmer, M. E. & O'Leary, D. P., 2001. Choosing regularization parameters in iterative methods for ill-posed problems, *SIAM journal on Matrix Analysis and Application*, **22**, 1204-1221.

Last, B. J. & Kubik, K., 1983. Compact gravity inversion, *Geophysics*, **48**, 713-721.

Li, Y. & Oldenburg, D. W., 1996. 3-D inversion of magnetic data, *Geophysics*, **61**, 394-408.

Li, Y. & Oldenburg, D. W., 1998. 3-D inversion of gravity data,*Geophysics*, **63**, 109-119.

Loke, M. H., Acworth, I. & Dahlin, T., 2003. A comparison of smooth and blocky inversion methods in 2D electrical imaging surveys, *Exploration Geophysics*, **34**, 182-187.

Marquardt, D. W., 1970. Generalized inverses, ridge regression, biased linear estimation, and nonlinear estimation, *Technometrics*, **12(3)**, 591-612.

Mead, J. L. & Renaut, R. A., 2009. A Newton root-finding algorithm for estimating the regularization parameter for solving ill-conditioned least squares problems, *Inverse Problems*, **25**, 025002.

Morozov, V. A., 1966. On the solution of functional equations by the method of regularization, *Sov. Math. Dokl.*, **7**, 414-417.

Paige, C. C. & Saunders, M. A., 1982. LSQR: An algorithm for sparse linear equations and sparse least squares, *ACM Trans. Math. Software*, **8**, 43-71.

Paige, C. C. & Saunders, M. A., 1982. ALGORITHM 583 LSQR: Sparse linear equations and least squares problems, *ACM Trans. Math. Software*, **8**, 195-209.

Portniaguine, O. & Zhdanov, M. S., 1999. Focusing geophysical inversion images, *Geophysics*, **64**, 874-887

Renaut, R. A., Hnetynková, I. & Mead, J. L., 2010. Regularization parameter estimation for large scale Tikhonov regularization using a priori information, *Computational Statistics and Data Analysis* **54(12)**, 3430-3445.

Renaut, R. A., Vatankhah, S. & Ardestani, V. E., 2015. Hybrid and iteratively reweighted regularization by unbiased predictive risk and weighted GCV for projected systems, `http://arxiv.org/abs/1509.00096`, September 2015, submitted.

Sun, J. & Li, Y., 2014. Adaptive L_p inversion for simultaneous recovery of both blocky and smooth features in geophysical model, *Geophys. J. Int*, **197**, 882-899.

Vatankhah, S., Ardestani, V. E. & Renaut, R. A., 2014a. Automatic estimation of the regularization parameter in 2-D focusing gravity inversion: application of the method to the Safo manganese mine in northwest of Iran, *Journal Of Geophysics and Engineering*, **11**, 045001.

Vatankhah, S., Ardestani, V. E. & Renaut, R. A., 2015. Application of the χ^2 principle and unbiased predictive risk estimator for determining the regularization parameter in 3D focusing gravity inversion, *Geophys. J. Int.*, **200**, 265-277.

Vatankhah, S., Renaut, R. A. & Ardestani, V. E., 2014b. Regularization parameter estimation for underdetermined problems by the χ^2 principle with application to 2D focusing gravity inversion, *Inverse Problems*, **30**, 085002.

Vogel, C. R., 2002. *Computational Methods for Inverse Problems*, SIAM Frontiers in Applied Mathematics, SIAM Philadelphia U.S.A.

Voronin, S., 2012. *Regularization of Linear Systems With Sparsity Constraints With Application to Large Scale Inverse Problems*, PhD thesis, Princeton University, U.S.A.

Wohlberg, B. & Rodriguez, P. 2007. An iteratively reweighted norm algorithm for minimization of total variation functionals, *IEEE Signal Processing Letters*, **14** 948–951.

APPENDIX A: SOLUTION USING SINGULAR VALUE DECOMPOSITION

Suppose $m^* = min(m, n)$ and the SVD of matrix $\tilde{\tilde{G}} \in \mathcal{R}^{m\times n}$ is given by $\tilde{\tilde{G}} = U\Sigma V^T$, where the singular values are ordered $\sigma_1 \geq \sigma_2 \geq \ldots \geq \sigma_{m^*} > 0$, and occur on the diagonal of $\Sigma \in \mathcal{R}^{m\times n}$ with $n-m$ zero columns (when $m < n$) or $m-n$ zero rows (when $m > n$), using the full definition of the SVD, (Golub & van Loan 1996). $U \in \mathcal{R}^{m\times m}$, and $V \in \mathcal{R}^{n\times n}$ are orthogonal matrices with columns denoted by $\mathbf{u}_i$ and $\mathbf{v}_i$. Then the solution of (10) is given by

$$\mathbf{h}(\alpha) = \sum_{i=1}^{m^*} \frac{\sigma_i^2}{\sigma_i^2 + \alpha^2} \frac{\mathbf{u}_i^T \tilde{\mathbf{r}}}{\sigma_i} \mathbf{v}_i \tag{A.1}$$

For the projected problem $B_t \in \mathcal{R}^{(t+1)\times t}$, i.e. $m > n$, and the expression still applies to give the solution of (16) with $\|\tilde{\mathbf{r}}\|_2 \mathbf{e}_{t+1}$ replacing $\tilde{\mathbf{r}}$, ζ replacing α, γ_i replacing σ_i and $m^* = t$ in (A.1).

APPENDIX B: REGULARIZATION PARAMETER ESTIMATION

The UPRE functional for determining α in the Tikhonov functional (9) with system matrix $\tilde{\tilde{G}}$ is expressible using the SVD for $\tilde{\tilde{G}}$

$$U(\alpha) = \sum_{i=1}^{m^*} \left(\frac{1}{\sigma_i^2 \alpha^{-2} + 1} \right)^2 \left(\mathbf{u}_i^T \tilde{\mathbf{r}} \right)^2 + 2 \left(\sum_{i=1}^{m^*} \frac{\sigma_i^2}{\sigma_i^2 + \alpha^2} \right) - m.$$

In the same way the UPRE functional for the projected problem (15) is given by

$$U(\zeta) = \sum_{i=1}^{t} \left(\frac{1}{\gamma_i^2 \zeta^{-2} + 1} \right)^2 \left(\mathbf{u}_i^T (\|\tilde{\mathbf{r}}\|_2 \mathbf{e}_{t+1}) \right)^2 + \sum_{i=t+1}^{t+1} \left(\mathbf{u}_i^T (\|\tilde{\mathbf{r}}\|_2 \mathbf{e}_{t+1}) \right)^2 + 2 \left(\sum_{i=1}^{t} \frac{\gamma_i^2}{\gamma_i^2 + \zeta^2} \right) - (t+1).$$

Then, for truncated UPRE, t is replaced by $t_{\text{trunc}} < t$ so that the terms from t_{trunc} to t are ignored, corresponding to dealing with these as constant with respect to the minimization of $U(\zeta)$.